Uncertainties of fluxes and $^{13}C/^{12}C$ ratios of atmospheric reactive gases emissions

Sergey Gromov[1,2], Carl A. M. Brenninkmeijer[1] and Patrick Jöckel[3]

[1] Max Planck Institute for Chemistry, Mainz
5 [2] Institute of Global Climate and Ecology (Roshydromet and RAS), Moscow
[3] Deutsches Zentrum für Luft- und Raumfahrt (DLR), Institut für Physik der Atmosphäre, Oberpfaffenhofen, Weßling

Correspondence to: Sergey Gromov (sergey.gromov@mpic.de)

Abstract. We provide a comprehensive review of the proxy data on the $^{13}C/^{12}C$ ratios and uncertainties of emissions of reactive carbonaceous compounds into the atmosphere, with a focus on CO sources. Based on an evaluated setup of the
10 EMAC model, we derive the isotope-resolved dataset of its emission inventory for the 1997−2005 period. Additionally, we revisit the calculus required for the correct derivation of uncertainties associated with isotope ratios of emission fluxes. The resulting $\delta^{13}C$ of overall surface CO emission in 2000 of $-(25.2\pm0.7)\,‰$ is in line with previous bottom-up estimates and a factor of two less uncertain. In contrast to this, we find that uncertainties of the respective inverse modelling estimates may be substantially larger due to the correlated nature of their derivation. We reckon the $\delta^{13}C$ values of surface emissions of
15 higher hydrocarbons being within $-24\,‰$ to $-27\,‰$ (uncertainty typically below $\pm1\,‰$), with an exception of isoprene and methanol emissions being close to $-30\,‰$ and $-60\,‰$, respectively. The isotope signature of ethane surface emission coincides with earlier estimates, however integrating very different source inputs. $\delta^{13}C$ values are reported relative to V-PDB.

1 Introduction

20 [1] Next to the kinetic chemistry implementation, magnitude and distribution of emissions of airborne compounds constitute perhaps the most crucial aspect of a modelling system dealing with the chemical state of Earth's atmosphere. A consistent emission setup, in turn, requires (i) a careful selection of the emission inventories, (ii) adequate approaches to special cases (*e.g.*, boundary conditions for the long-lived species) and, not less important, (iii) estimates of the pertinent uncertainties. The latter, typically being largest in comparison to the other sources of error in the model (such as for instance reaction rate
25 coefficients), are often disregarded, when the resulting simulated mixing ratios are reported. Often the inferred variation (temporal or spatial) of the species' abundance is quoted, which, however, does not represent an adequate uncertainty estimate. The situation complicates, if the isotope-resolved emissions (*i.e.*, fluxes separated using the information on the isotope ratios of the emitted compounds) are to be used. For instance, which factors determine a particular emission source isotope ratio? How do these (and their respective uncertainties) influence the uncertainties of the underlying fluxes? And finally,
30 what is the contribution of the emissions uncertainties to the overall uncertainties of the simulated mixing/isotope ratios?

[2] The above mentioned issues and questions interested us in the course the implementation of a fully $^{13}C/^{12}C$-resolved comprehensive trace gas atmospheric chemistry study with the **ECHAM/MESS**y **A**tmospheric **C**hemistry (EMAC) model (Jöckel *et al.*, 2006; Jöckel *et al.*, 2010), particularly for the stable carbon isotope extension of its emission setup, which we communicate in this paper. The reader is referred to the preceding phases of this model development, *viz.* the isotope extension of the kinetic chemistry submodel MECCA (**M**odule **E**fficiently **C**alculating the **C**hemistry of the **A**tmosphere) and its application to simulating the carbon and oxygen isotope composition of gas-phase constituents within the CAABA (**C**hemistry **A**s **A B**oxmodel **A**pplication) atmospheric box-model (Sander *et al.*, 2011; Gromov *et al.*, 2010). Both EMAC (which embodies an atmospheric chemistry general circulation model, AC-GCM) and CAABA serve as base models within the **M**odular **E**arth **S**ubmodel **Sy**stem (MESSy, Jöckel *et al.*, 2005) we employ. The overarching aim of our studies is a consistent simulation of the isotopic composition of atmospheric carbon monoxide (CO). A handful of modelling studies dedicated to CO isotopes exist to date (see the review by Brenninkmeijer *et al.*, 1999) and has proven to yield deeper insights into its budget, however leaving questions on missing atmospheric ^{13}CO in models (see Sect. 4). We therefore attempt to revisit this issue in a detailed and more comprehensive framework of the EMAC model, which we will communicate in subsequent papers. In addition to CO, the current study provides a bottom-up assessment of the emission $^{13}C/^{12}C$ isotope ratios for the suite of other carbonaceous compounds, the information that we believe will be useful for other isotope-enabled (modelling) studies focussing on these. For further information we refer to Brenninkmeijer *et al.* (2003), Goldstein and Shaw (2003) and Gensch *et al.* (2014) who review the benefits of using stable isotope ratios in atmospheric trace gases we consider in this work.

[3] The manuscript consists of three main parts. In the first part (Sect. 2), we briefly reiterate the implementation of the trace gas emissions in the evaluation setup of the EMAC model (MESSy Development Cycle 2, Jöckel *et al.*, 2010, referred hereafter to as "EVAL$_2$") and supplement it with the formulation used to separate isotope emission fluxes. Furthermore, we derive some practical approaches for calculating combined flux/isotope ratio uncertainties of emissions in Sect. 2.2. The second part (Sect. 3) revisits proxies for signatures ($^{13}C/^{12}C$ isotope ratios) of particular emission sources for CO, non-methane hydrocarbons (NMHCs), biogenic volatile organic (VOCs) and other carbonaceous compounds represented by EMAC. Special focus is on CO (the tracer of our primary interest) and its precursors. Finally, in the last part (Sect. 4) we summarise the results and discuss our estimates in comparison with previous studies. We recapitulate our results in Sect. 5 with concluding remarks.

2 Emission processes in EMAC

[4] The emission of trace gases in EMAC is treated by the submodels OFFEMIS (formerly OFFLEM), ONEMIS (formerly ONLEM) and TNUDGE, which embody **off-l**ine and **on-l**ine **em**ission processes, and a pseudo-emission approach (**t**racer **nudg**ing), respectively, as detailed by Kerkweg *et al.* (2006). The off-line emission process embodies a prescribed (precalculated) tracer flux into the atmospheric reservoir at the surface layer(s) or, for instance for the emission from air transpor-

tation sector, at the respective altitudes. This type of emission does not require a parameterisation dependent on the model parameters. The EVAL$_2$ setup includes the emissions from datasets comprising the following categories:

65
    – anthropogenic emissions, based on the EDGAR emission inventory (detailed in Sect. 3.1),

    – biomass burning emissions (GFED project database, 2nd version, see Sect. 3.2), and

    – biogenic emissions based on the OLSEN/GEIA databases (see Sect. 3.3, respectively).

Various key assumptions determine the emission isotopic signatures. Depending on the specific emission category, each of the datasets requires separate pre-processing for the isotopic extension. These are described in Sects. 3.1 to 3.5, respectively.

70
[5] The on-line emissions, in contrast, are calculated during the runtime and require some of the model variables (*e.g.* surface temperature or precipitation) for calculating the resulting emission flux at the given model time step. For example, online emission suits for parameterisation of the trace gas emissions related to the biosphere-atmosphere interaction processes. In particular, the EVAL$_2$ setup includes the online emissions of VOCs (isoprene/monoterpenes) from plants (see below, Sect. 3.3.1), which were scaled to achieve net yearly emissions of 305−340 Tg(C) of isoprene, respectively (see Pozzer *et al.*,

75
2007, Supplementary Material). With this adjustment, more realistic mixing ratios of isoprene in the boundary layer are achieved in EMAC simulations.

[6] At last, the pseudo-emission approach (tracer nudging) is a technique performing the relaxation of the mixing ratios of sufficiently long-lived tracers towards prescribed (in space/time) fields. In the EVAL$_2$ setup, these are the zonal averages of the observed mixing ratios of CH_4, chlorinated hydrocarbons (CH_3CCl_3, CCl_4, CH_3Cl) and CO_2 which are used as the lower

80
boundary conditions (surface layer) in the model. The isotopic separation of these pseudo-emission fields is described below in Sect. 3.5.

[7] Further details of the emission processes implementation in EMAC and the corresponding model parameterisations are given by Kerkweg *et al.* (2006), Jöckel *et al.* (2006), Pozzer *et al.* (2007), Pozzer *et al.* (2009) and Jöckel *et al.* (2010). In the next sections we describe chiefly the choice of the isotope emission signatures for the model setups including stable carbon

85
isotopes.

2.1 Individual fluxes of isotopologues

[8] The isotopic extension procedure consists of the separation of the total (*i.e.*, sum of the abundant and rare isotope bearing) species fluxes into the individual isotopologues fluxes accounting for the given isotopic ratio and thus the isotope content of a given species. Additionally, the consistency between the total flux and the sum of isotopically separated fluxes is

90
verified. The rare isotopologues fluxes are calculated by weighting the total species flux with the respective fractions $^{\text{rare},i}f$ according to

$$^{\text{rare},i}f = \frac{^{\text{rare},i}R \cdot q}{1+\sum_j {}^{\text{rare},j}R}, \quad {}^{i}R = \left(\delta^i + 1\right) \cdot {}^{i}R_{\text{st}}. \tag{1}$$

Here, q is the number of atoms of the selected isotope in a given species' molecule, index j cycles all rare isotopologues (*e.g.*, ^{13}CO for stable C, $C^{17}O$ and $C^{18}O$ for stable O substitutions of CO), ^iR is the isotopic ratio of a particular isotope i in the flux, $^iR_{st}$ is the reference standard isotope ratio, respectively. When accounting for multiple rare isotopes, all ratios are required for the correct calculation of the resulting fraction of each of the isotopologues. The abundant isotopologue flux fraction, in turn, is calculated as

$$^{abun}f = 1 - \sum_j {}^{rare,j}f , \tag{2}$$

thus assuring that the sum of isotopically separated fluxes of the abundant and rare isotopologues equals the total flux value. The resulting fluxes F of the regular species and its isotopologues are:

$$\begin{cases} {}^{abun}F = F \cdot {}^{abun}f \\ {}^{rare,i}F = F \cdot {}^{rare,i}f \\ F \equiv {}^{abun}F + \sum_j {}^{rare,j}F \end{cases}, \tag{3}$$

For the sake of clarity, the molecular fractions f above are calculated plainly from the atomic content q and the isotopic ratios. The isotopic compositions of the emission fluxes, nevertheless, are conventionally (and within this study) reported using delta values δ^i, which relate the isotope ratio ^iR and the standard ratio $^iR_{st}$ in (1). For expressing $\delta^{13}C$ values (or "signatures") the V-PDB scale with $^{13C}R_{st}$ of 11237.2×10^{-6} (Craig, 1957) is used hereinafter (see Appendix for details on choosing the $^{13C}R_{st}$ value).

[9] During the isotopic extension of the emission data, the preparation tools import the regular (total) emission fields (usually provided in netCDF format (http://www.unidata.ucar.edu/software/netcdf) with the flux values in units of molecules $m^{-2}\,s^{-1}$), process these according to the given isotopic signatures and output fields containing the individual isotopologue fluxes. These in turn are read in by the model data import interface and utilised in a conventional way by the emission submodels (*e.g.*, OFFEMIS). Depending on the source data used, the spatial resolution of the emission datasets varies. The input fields are transformed to the model grid during the model integration with the help of the NCREGRID submodel (Jöckel, 2006), which provides the consistent (flux-conserving) re-gridding algorithm.

2.2 Emission uncertainties analysis

[10] It is desirable to estimate the uncertainties associated with the emission signatures for the subsequent analysis of the modelling results, particularly in view of comparison with observational data. However, deriving the isotope composition uncertainties for composites of the various different sources with superimposed individual isotopic ratios is an intricate task. First, it should be clear how the uncertainties of the isotopic ratios are related, particularly in view of summing of several compartments (*e.g.* emission fluxes from different sources), all with their individual uncertainties for abundance and isotope composition. Second, the uncertainties associated with the *amounts* being summed are expected to influence the combined uncertainty of the *ratio* of the final aggregate, as a consequence of the law of error propagation. Even if the isotopic signature

of each share (*i.e.* particular emission type) is determined (ideally) precisely, the non-zero uncertainties associated with the amounts of each share (*i.e.*, emission fluxes) impose a non-zero uncertainty on the final isotopic signature of the total (emission). The approaches to calculate combined emission and its isotope composition uncertainties are only sparingly documented in the literature, therefore they are derived below. The following analysis is based on the common practical fundament of uncertainties as described, for instance, by Drosg (2009) and by Criss (1999).

[11] Foremost, it is expedient to switch from using the relative isotopic composition to the actual equivalent ratio, *i.e.* from δ^i to ^iR. The use of delta variables would introduce impermeable complexities in subsequent calculations because in contrast to ratios, it is much more difficult to relate delta-values to extensive quantities such as fluxes. The relation of the uncertainty $\langle \delta^i \rangle$ reported for the delta value δ^i to the uncertainty $\langle ^iR \rangle$ of the corresponding ratio ^iR is

$$\langle ^iR \rangle = \left(\frac{d\delta^i}{d\,^iR} \right) \Delta \delta^i = {}^iR_{st} \cdot \langle \delta^i \rangle \,. \tag{4}$$

Here and further, the notation from Eqs. (1)−(3) is applied. For clarity the angle brackets $\langle \ \rangle$ are introduced in place of conventional "Δ" to denote the uncertainty values. The delta-value uncertainty is linearly proportional to the ratio uncertainty with the reference standard ratio being the proportionality factor. The total emission flux F_e of a given species is an integral of the particular emission source fluxes F_s. Employing the same notation, the values of F_e and its isotopic ratio ^iR_e are

$$F_e = \sum_s F_s,$$
$$^iR_e = \varphi \sum_s {}^iR_s \cdot F_s, \qquad \varphi \equiv \left(\sum_s F_s \right)^{-1} . \tag{5}$$

The summation in Eq. (5) is performed over the emission sources using index *s*, φ is introduced for the sake of notation simplification. Noteworthy, source fluxes F_s cannot be used if the summation is done over several species with varying isotope element count in the molecule. In that case, fluxes and their individual uncertainties $\langle F_s \rangle$ must be reduced to mole or mass fractions of the element of interest, *e.g.* kg(C) yr^{-1} (see Criss (1999), Sect. 1.4 for details).

[12] It is important for the applied method to differentiate whether or not the uncertainties associated with the magnitude of the individual emission fluxes and/or isotope ratios are *correlated*, that is, the various given estimates depend on each other. Examples of such are inverse modelling and other "top-down" approaches which may intrinsically correlate the fluxes from different emission sources by distributing their shares to the given (isotope mass-balanced) integral. Using any inverse modelling framework commonly requires the analysis of the posterior solution distribution, *e.g.*, via an analytical solution, a systematic study of cases or a Monte Carlo study (see the review in Enting, 2002, Sect. 3.2). As pointed out by Tarantola (2005) (Sect. 3.3), at least a trivial estimate of the uncertainties correlation is always possible. We note beforehand that no such estimates were provided among the inverse modelling studies regarded here (see below Sect. 4). Therefore, we are to gauge the upper limit (the "worst case") of their uncertainties by assuming them correlated. The "bottom-up" estimates, on the contrary, are typically derived using independent proxies (*e.g.*, country fuel usage statistics, satellite-derived mass of burned

matter). Often uncertainties of assumptions (for example, if the emission comes predominantly from a particular plant mate-rial characterised by the distinct isotope signature) cannot be quantified using strict mathematical apparatus, hence should be analysed in a sensitivity framework. In other cases, the combined uncertainty accounting for the error propagation is calcu-lated using the total differential of the function describing the product, in forms which are different for the correlated and uncorrelated estimates. Thus, the combined uncertainty $\langle F_e \rangle$ of the total emission F_e in Eq. (5) expressed through the uncer-tainties of correlated (inferred "top-down") components $\langle F_s \rangle$ of individual sources F_s is

$$\langle F_e \rangle = \sum_s \left| \frac{\partial F_e}{\partial F_s} \right| \cdot \langle F_s \rangle = \sum_s \langle F_s \rangle \tag{6}$$

i.e., a simple (linear) addition of the individual uncertainties. In the case of uncorrelated (estimated "bottom-up") total flux components, the resulting combined uncertainty is derived using the quadratic form of Eq. (6), which yields the square root of the sum of squared components $\langle F_s \rangle$, respectively:

$$\langle F_e \rangle = \sqrt{\sum_s \langle F_s \rangle^2} \; . \tag{7}$$

Analogously, the combined uncertainty $\langle R_e \rangle$ for the resulting total emission isotope ratio R_e is calculated from both, flux components ($F_s \pm \langle F_s \rangle$) and ratio components ($R_s \pm \langle R_s \rangle$), as (index n varies similarly to s, enumerating the sources)

$$\langle {}^i R_e \rangle = \sum_s \left(\left| \frac{\partial\, {}^i R_e}{\partial F_s} \right| \cdot \langle F_s \rangle + \left| \frac{\partial\, {}^i R_e}{\partial R_s} \right| \cdot \langle {}^i R_s \rangle \right) =$$
$$= \sum_s \left(\left| \varphi^2 \cdot \sum_n F_n \left({}^i R_s - {}^i R_n \right) \right| \cdot \langle F_s \rangle + \left| \varphi \cdot F_s \right| \cdot \langle {}^i R_s \rangle \right) \tag{8}$$

for the correlated case. The first term of the final sum in Eq. (8) describes the uncertainty in the isotope ratio arising purely from the uncertainty in emission strengths modified by the difference in the isotopic ratios between each pair of sources. The second term adds the uncertainties of the source isotope ratios weighted by the corresponding emission fluxes. In the case of uncorrelated estimates, the quadratic form of Eq. (8) yields the square root of a similar expression incorporating the above-mentioned terms squared:

$$\langle {}^i R_e \rangle = \sqrt{\sum_s \left(\left(\varphi^2 \cdot \sum_n F_n \left({}^i R_s - {}^i R_n \right) \right)^2 \cdot \langle F_s \rangle^2 + \atop + \left(\varphi \cdot F_s \right)^2 \cdot \langle {}^i R_s \rangle^2 \right)} \; . \tag{9}$$

Eqs. (6)−(9) can be employed for the uncertainty estimation of any given combination of isotopic compartments, referring only to their abundances (or fluxes) and isotopic ratios. We remark here that using Eqs. (6)−(9) implies that the final com-bined uncertainties have a normal distribution about their mean values (*i.e.*, standard deviations), despite that such may not be the case for individual emission flux estimates. Under the assumption of symmetricity for all individual uncertainties in-

volved, however, normally distributed $\langle^i R_e \rangle$ will be indeed the consequence of the law of uncertainty propagation (see D'Agostini, 2004 for details).

3 Proxies of emissions and their ^{13}C/^{12}C ratios

3.1 Anthropogenic emissions

[13] The anthropogenic emissions in EVAL$_2$ are based on the EDGAR database (version 3.2 "Fast Track 2000" (32FT2000), van Aardenne *et al.*, 2005) as detailed by Pozzer *et al.* (2007). This inventory was compiled for the year 2000. It is noteworthy that, despite its complex structure (the emission is distributed to tens of various categories, or "sectors"), the database has no seasonality, *i.e.* spatially distributed emission fluxes composing the emission are constant throughout the year. The inventory comprises approximately 40 sectors referring to the different anthropogenic emission sources (summarised in Table 1), which enables to assign characteristic isotopic signatures individually to each sector. The influx is distributed to the surface and several near-surface model layers, depending on the emitted species and the emission sector. This serves to account for specific sources that deliver the pollutants to the various effective altitudes. The majority of sectors are associated with the surface and adjacent layers representing 45 m and 140 m heights. The sources from power generation, industrial fuel usage and waste treatment sectors are represented with the various plume updrafts distributed to the higher layers (spanning from 240 m to 800 m above the ground). The detailed anthropogenic emission setup and vertical distribution of the emission heights is described by Pozzer *et al.* (2009).

[14] Table 1 lists the carbon isotopic signatures for CO and other emitted compounds assigned to the particular sector for anthropogenic emissions. Unfortunately, to date the information in the literature on the measured isotopic compositions of the different emitted compounds is scarce, particularly for NMHCs and other VOCs. Therefore, here the choice for the unknown signatures will follow the EDGAR categorisation, assuming the emission source material (*e.g.* crops, bio- or fossil fuels) and its characteristic processing (generally either biomass burning or high-temperature combustion) to determine the resulting isotopic ratio of the emitted tracer.

[15] The least uncertain signature is for fossil fuel usage, most of which is on account of the transportation sectors. It is associated with an average characteristic composition of $-27.5\,‰$ in δ^{13}C, as reported for the world average engine exhaust CO by Stevens *et al.* (1972) and used as a proxy value here. Although quite diverse emitted CO isotope signatures were measured for various engine/fuel types (Kato *et al.*, 1999a), any better assessment based on these signatures is not feasible, because the inventory does not provide the related information. The average value from Stevens *et al.* (1972), nonetheless, agrees with more recent estimates. Thus, from measurements of CO isotopic composition in two cites in Switzerland, Saurer *et al.* (2009) infer the δ^{13}C signature of the transportation source of $-(27.2\pm1.5)\,‰$, contrasting heavier CO emitted from local wood combustion sources. A similar transportation-emitted CO δ^{13}C average value ensues from the observations in a

Swiss highway tunnel study by Popa *et al.* (2014), *viz.* $-(27.5\pm0.6)\,‰$ (the average $\pm2\sigma$ of the two Keeling plot-derived source $\delta^{13}C$ signatures from the tunnel entrance and exit data is quoted).

[16] Statistically insignificant variability in emission isotope ratios for transportation-related sources of selected NMHCs has been reported by Rudolph *et al.* (2002) with the signatures for the majority of species equating to within the measurement precision of $2\,‰$ that of CO mentioned above. The exception of significant enrichment was found for ethyne (C_2H_2), which is not represented in the MECCA chemistry mechanism (as of $EVAL_2$ setup) and may potentially constitute an enriched, however, very moderate source (see, for example, Ho *et al.*, 2009). This is somewhat coherent with ^{13}C enrichments found to accompany ethyne formation during the burning process (Czapiewski *et al.*, 2002). We refer the reader to Gensch *et al.*, 2014 for further details and a comprehensive review on wide range of NMHC/VOC compounds. Altogether it is generally recognised that the fossil-related sources reflect the average isotopic ratios of the precursor crude oils. The aircraft emissions are associated with this source as well. However, the corresponding EDGAR emission (class F57) is replaced by the inventory compiled by Schmitt and Brunner (1997) in $EVAL_2$.

[17] In analogy to the fuel combustion category (sectors "F"), the same isotopic signature ($-27.5\,‰$) is used for the industrial category (sectors "I"). It is expedient to assume that those sources represent dominantly the fossil nature of the precursor carbon, as the emission is mainly associated with the combustion of fuels in the majority of the industrial processes. An example is iron and steel production (sector I10), where CO is emitted concomitantly during the thermal processing of the product in the furnaces (IISI, 2004). On the other hand, the influence of industrial sectors on the resulting emission signature should be minor, taking into account their small share in the overall anthropogenic emission. The comparison of the contributions of each EDGAR sector in case of CO emission is presented in Fig. 1. Notably, the largest fluxes are associated with sectors B40 (biofuel consumption in the residential/commercial sector) and F51 (non-CO_2 combustion emissions from road transport), thus the input shares of these two sectors are decisive for the overall isotopic composition of CO in EDGAR. The total emission associated with industrial sectors amounts to $34.5\,Tg(CO)\,yr^{-1}$, that comprises approximately $6.3\,\%$ of the total anthropogenic source.

[18] The less certain isotope signatures are associated, in turn, with the biofuel use (sectors "B") because of large uncertainties associated with the source influx estimates and somewhat unclear definition of this category itself. Although we reckon that "biofuel use" in EDGAR refers to predominantly combustion of fuel wood and vegetable oils, the category includes industrial activities that may imply usage of fuels (*e.g.,* liquid, gas, solid) *produced* from biomass (Olivier *et al.*, 2002). To eliminate a potentially wrong association with the biofuel category, we discuss the isotope signatures of the woodfuel and waste/residue crops sources under the "biomass burning" category below. We remark that this activity comprises likely the major fraction of the "biofuel use" emissions related to heating and cooking in Asian and African regions (Yevich and Logan, 2003). No detailed information is available about the biofuel production and use in other regions, however, particularly for the period the EDGAR inventory was compiled for. Likewise, there are no specific measurements of the isotopic signatures of CO and other NMHCs/VOCs from biofuel sources reported yet (Goldstein and Shaw, 2003). These mainly

comprise the use (primarily by combustion) of vegetable oil- and biomass-derived fuels, of which biodiesel and ethanol constitute the major parts (Demirbas, 2008). Although ethanol is included in the "biofuel combustion" category in EDGAR, neither the proportion of ethanol/biodiesel fuel sources nor the origin of precursor biogenic material is reflected in the inventory. A rough estimate of the isotopic signature is feasible nonetheless, assuming a certain average composition of the source biomass and negligible isotope effects accompanying the emission. On average, plant material is enriched in ^{13}C with respect to fossil fuels and can be considered as a composite of the carbon originating from two cardinal kinds of plant species, namely C_3 and C_4 plants (explained in detail in the following, see Sect. 3.3.1). Briefly, the isotopic compositions of those differ conspicuously owing to the differences in the photosynthesis mechanisms, yielding typical compositions of −27‰ for C_3 plants and −12‰ for C_4 plants (see, *e.g.*, Dawson *et al.*, 2002). The expected composition of the mixture is hence constrained by these values. Within the current study we follow Emmons *et al.* (2004) and adopt the value of −25‰, which corresponds to an approximate 4:1 ratio of C_3 to C_4 plant material. There are, however, estimates that report a significantly higher fraction of C_4 plants being used in global biofuel production. Thus, O'Connor (2009) quote the source plants species used for ethanol and biodiesel production. Whilst biodiesel is mainly produced from C_3 species like soy, rapeseed, canola and oil palm tree, ethanol is predominantly manufactured from corn and sugarcane, which are C_4 crops. Projecting this partitioning on the gross production rates for the year 2000 (Demirbas, 2009) of $156 \cdot 10^8$ and $9.7 \cdot 10^8$ litres for ethanol and biodiesel, respectively, will yield a rather high value for the average emission signature of −12.9‰ for these fuels. Here, the fractionation associated with the fermentation process during the ethanol production is assumed to be negligible, although a few studies (Vallet *et al.*, 1998; Zhang *et al.*, 2003) indicate that the biogenic ethanol may be even slightly enriched with respect to the source material. A substitution of the reference biofuel δ^{13}C signature of −25‰ with the above derived value of −12.9‰ will result in an unlikely strong increase (greater than +8‰) in the overall surface CO emission δ^{13}C in East Asia and Central Africa, compared to that for Europe and North America (+1.6‰ and +1.1‰, respectively), where biofuel is being less extensively used. On a global scale, this enhancement reaches +4.6‰, zonally distributed as +6.1‰ and +3.8‰/+2.1‰ in the tropics and extratropical northern/southern hemispheres, respectively. The sensitivities to such substitution for the δ^{13}C of NMHCs/VOCs emissions are lower, *viz.* +4.9‰ (East Asia) and +2.8‰ (Central Africa) *vs.* +1.0‰ and +0.8‰ for Europe and North America, respectively, with a global average of +1.6‰. This rough analysis suggests that the sensitivity of simulated CO and NMHCs δ^{13}C to biofuel ^{13}C/^{12}C signature for Europe and North America will be likely below the (rather large) uncertainties associated with the biofuel category emission fluxes and isotope ratios itself (see also Sect. 3.6 below).

[19] The original biomass burning emission inventory of the EDGAR database (referring to land use, sectors "L") in the current setup is substituted by the more comprehensive GFED inventory described in the following section, with the exception of the agricultural waste burning sector (L43), which is not included in GFED. The emission δ^{13}C signature of −22.2‰ is assigned to this source using the average composition of the burned material estimated for 2000 by Randerson *et al.* (2005). They use the C_3/C_4 ratio of the burned vegetation inferred with the help of a vegetation-inclusive inversion-adjusted model and comparison with observed CO_2 isotope ratios. A different signature of −21.3‰ for CO is used, following the estimation similarly based on plant distribution, fuel loads and neglecting concomitant fractionations as described by Conny (1998). The

estimates of burned plant composition by Randerson *et al.* (2005) do not consider the potential kinetic isotope effects that may escort biomass burning emission for various tracers.

[20] Czapiewski *et al.* (2002) and later Komatsu *et al.* (2005) and Nara *et al.* (2006) report that δ^{13}C of the major NMHCs
275 emitted from biomass burning generally follows that of the fuel burnt, and the measurements did not reveal significant additional fractionations associated with the formation processes. Consequently, here (and further for the GFED data) the ^{13}C isotope fractionation escorting burning process is assumed to be negligible. On the contrary, the combustion conditions play a key role in formation of CO during the biomass burning: Normal (+0.5‰ to +3.6‰) and inverse (−2.1‰ to −6.8‰) ^{13}C fractionations were found to escort flaming and smouldering burning stages, respectively, with a further complex dependency on the burnt plant type (Kato *et al.*, 1999b). The average composition of CO is rather expected to be depleted with respect to the source fuel, since CO emission is expected to be favoured in the smouldering phase (Yokelson *et al.*, 1997). Unfortunately, the representation of the combustion stages in the emission data is limited; hence, one can provide only a qualitative estimate of the isotope effect (depletion). The quantitative estimates of the contributions from various stages (like, for instance, in the modelling study by Soja *et al.*, 2004) could be improved with the use of the isotopic composition in this case. Conclusively, in contrast to the primary biomass burning sources, the emissions from the sector L43 induce a minor influence on the average CO emission signature, accounting for a total of 16.3 Tg(CO) per year (less than 3 % of the total anthropogenic emission). In an analogous way, the waste treatment-related sources (sectors "W") are assigned to a slightly enriched (compared to the average fossil fuel carbon) composition of −24‰ using the ratio of the biological to fossil carbon for waste incineration from Johnke (2000). It is assumed that the waste treatment category refers to the waste incineration processes mainly.

[21] Table 2 lists the anthropogenic emissions and the compositions for the EDGAR database. The emissions for CO sum up to almost 550 Tg yr^{-1}, while the overall influx for the other trace gases amounts to approximately 106 Tg(C) yr^{-1}. The mixing of the compositions of the main CO contributors, bio- and fossil fuel in proportion of about 250:280, respectively, yields the average composition of −26.15‰. This value is apparently sensitive to the assumed biofuel δ^{13}C signature. The influence of the biofuel sources is dominating for methanol, formaldehyde, formic acid, acetaldehyde and acetic acid, with values close to −25‰. Emitted alkanes and alkenes are enriched in ^{13}C similar to CO, with an increasing influence of the fossil fuel input towards the higher hydrocarbons. The spatial distribution of the δ^{13}C of anthropogenically emitted CO is depicted in Fig. 2, with the panels referring to the specific emission altitudes, as described above. The two lowermost layers subsume the majority of the emission sectors, including the shipping and biofuel-related sources (equally distributed to the layers) and fossil fuel sources (falling mainly in the surface layer). The emission signatures reflect the dominant biofuel emissions in Africa, eastern Asia and Oceania (panel a). In the second emission layer (panel b) the agricultural waste burning and waste incineration sources are reflected together with the biofuel emission. The overlying layers include the mixture of industrial and power generation sectors, with the latter prevailing in the top two layers.

3.2 Biomass burning emissions

[22] The biomass burning emission data is prepared from the ORNL DAAC Global Fire Emission Database (GFED), version 2.1 inventory (Randerson *et al.*, 2007, http://daac.ornl.gov/VEGETATION/guides/global_fire_emissions_v2.1.html), which is an updated and extended version of the initial GFED version 1 release (van der Werf *et al.*, 2006) used in the EVAL$_2$ setup (Pozzer *et al.*, 2009). In the current setup, monthly mean emission fields covering the period from 1997 to 2005 are used. The inventory includes emission fluxes for CO, NMHCs, nitrogen oxides (NO$_x$) and other species; in addition, the estimation of the C$_4$ plant carbon fraction of the burnt material is provided (Randerson *et al.*, 2005). The latter is used to assign the isotopic signatures to the emission fluxes, assuming negligible isotopic fractionation during the burning, except for methanol (CH$_3$OH), as discussed below. The resulting isotopologues fluxes are calculated as:

$$
\begin{cases}
\dfrac{^{13\mathrm{C}}F}{F} = \left(1 - f_{\mathrm{C}_4}\right)\dfrac{q \cdot R_{\mathrm{C}_3}}{R_{\mathrm{C}_3} + 1} + f_{\mathrm{C}_4}\dfrac{q \cdot R_{\mathrm{C}_4}}{R_{\mathrm{C}_4} + 1} \\[3mm]
\dfrac{^{12\mathrm{C}}F}{F} = \left(1 - f_{\mathrm{C}_4}\right)\dfrac{(1 - q) \cdot R_{\mathrm{C}_3} + 1}{R_{\mathrm{C}_3} + 1} + \\[3mm]
\qquad\quad + f_{\mathrm{C}_4}\dfrac{(1 - q) \cdot R_{\mathrm{C}_4} + 1}{R_{\mathrm{C}_4} + 1}
\end{cases}
\tag{10}
$$

The notation follows that from Eq. (1) and f_{C_4} denotes the fraction of the burnt C$_4$ plant material, F is the total emission flux. Ratios R_{C_3} and R_{C_4} refer to the ^{13}C isotope content associated with C$_3$ and C$_4$ plants, respectively; the corresponding isotopic signatures are discussed above. The emission is released into the near-surface model layer corresponding to 140 m height (see also Sect. 3.1).

[23] For the sake of comparison presented here, an averaged (ensemble mean) yearly biomass burning "climatology" was derived, referring to the 2000−2005 period of the original data. The "climatological" yearly average spatial distribution of a burnt C$_4$ biomass fraction and its translation into δ^{13}C values of the emission are presented in Fig. 3. The heaviest (*i.e.*, most enriched in ^{13}C) composition of the emission is associated with the grassland and savannah burning regions, where the C$_4$ crops are most abundant.

[24] In Fig. 4 the temporal evolution of the hemisphere-integrated CO emission from biomass burning is presented. The markedly intensified emission rates in 1997−1998 are attributed to the increased forest and peat fires due to the droughts induced by the strong El-Niño southern oscillation climate pattern in those years (ENSO, Dube, 2009). Such event is also notable (although less pronounced) for the years 2002−2003. Interestingly, ENSO activity is hardly reflected in the isotopic composition of the emission. However, the influence of the biomass source, especially important for its ^{13}C enriched composition in the tropics and southern hemisphere (SH), without doubt increases during El-Niño years. The variation of the emission flux δ^{13}C is twice as large in the northern hemisphere (NH) compared to that in the southern hemisphere. Such a difference arises from the large C$_3$ plant extent at the northern high latitudes and the pronounced seasonal fire cycle. The summer/fall extratropical fires in the NH occur predominantly in C$_3$ plant communities, mainly forests of an average −27‰ composition. In

the winter time the (sub)tropical sources take over enriching the emission to the maximum of $-19\,‰$ due to the large C_4 plant fraction burnt in Africa and Asia. In the SH, the spatial diversity of the C_3/C_4 ratio is smaller over the smaller land extent, and the average signature varies around $-24\,‰$ within $\pm1\,‰$ only.

[25] The annual average biomass burning emission rates for the relevant species are listed in Table 3. In contrast to CO and CH_3OH, all NMHCs/VOCs emitted possess an equal isotopic composition because the fluxes for carbonaceous species are principally derived from the same burned carbon emission proxy (van der Werf *et al.*, 2006). In order to obtain the individual tracer emission, the proxy is scaled with the corresponding emission factor (conventions and values from Andreae and Merlet, 2001 are used), but the spatial distribution of the emission, hence C_3/C_4 carbon ratio, is the same. The difference in average hemispheric $\delta^{13}C$ value amounts to $0.4\,‰$ with the heavier emission in the SH. Compared to NMHCs/VOCs, the CO emission flux mapped onto the same burnt C_4 plant fraction results in a slightly heavier ($+0.3\,‰$ in $\delta^{13}C$) average composition in GFED. An exceptional case amongst NMHCs is CH_3OH which emitted significantly depleted, as shown by Yamada *et al.* (2009). They attribute changes to the emission $\delta^{13}C$ signature to the variations in the fraction of the precursor material (pectin *vs.* lignin methoxy pools, see also Keppler *et al.*, 2004) and kinetic effects in loss processes. The overall depletion of CH_3OH w.r.t. the plant material is found to linearly correlate with the fire modified combustion efficiency (MCE $= \Delta CO_2/(\Delta CO+\Delta CO_2)$, "$\Delta$" denotes trace gas concentration enchancement due to emission). Depletions of $-(20-6)‰$ were measured withing the studied range of MCE values of $(85-98)\,\%$. Employing the relation provided by Yamada *et al.* (2009) and GFED-derived MCE we estimate the global average depletion of CH_3OH w.r.t. the plant material of $-(12.4\pm0.8)‰$, which corresponds to the average MCE value of $(92.3\pm0.7)\,\%$. The resulting methanol BB emission signature of $-(36.9\pm2.2)\,‰$ in EMAC compares well with $-(33\pm16)\,‰$ inferred by Yamada *et al.* (2009). Notably, the GFED v2.1 inventory provides the combustion completeness parameter (CC), the estimate of the fraction of the actual fuel load combusted. Being similar to the MCE, CC might better reflect the burning stage conditions (*i.e.* flaming or smouldering phases). Unfortunately, the correspondence between these parameters is not assessed to date; future applications of combustion completeness accounting for the kinetic isotope effects escorting biomass burning would be of great benefit.

3.3 Biogenic emissions

[26] The biogenic emissions represent the discharge of organic species into the atmosphere associated with biosphere activity, particularly oceanic, soil and plant emissions. The current biogenic emission setup in $EVAL_2$ follows Guenther *et al.* (1995) as described by Kerkweg *et al.* (2006), and comprises two parts for offline and online emissions, respectively (see the introduction in Sect. 2). The offline part was reassessed by Pozzer *et al.* (2007) and prescribes the emission for the large set of NMHCs/VOCs, excluding isoprene/monoterpenes emissions, which are calculated online. The data have a temporal resolution of one month, thus approximating the emission seasonal variation with no interannual variability. The emission is applied to the lowermost model layer. The CO emission comprises in-place oxidation of some (non-industrial) hydrocarbons not accounted for in the applied MECCA chemistry (*i.e.* higher alkenes (C>3), terpene products other than acetone, higher aldehydes) and some direct CO emissions by vegetation and decaying plant matter. The oceanic CO emission strengths

 (monthly zonal distribution) are taken from Bates *et al.* (1995). No biogenic emissions for formaldehyde (HCHO), acetalde-hyde (CH_3CHO) and higher ketones (represented by methylethylketone (MEK) in MECCA) are included. The total annual emission strengths for CO and NMHCs/VOCs with the corresponding average compositions are listed in Table 4.

[27] For the majority of the species, plant activity is the dominating biogenic emission. For a few species, *viz.* acetic acid (CH_3COOH), formic acid (HCOOH) and ethene (C_2H_4), the emission from the soils is estimated to be of comparable magni-

 tude to the plants source (Kesselmeier and Staudt, 1999). Unfortunately, hardly any measurements or estimates of the iso-topic composition of the soil-emitted carbon of these VOCs are available. The composition of precursor soil organic matter is also not well known (Boutton, 1991). Regarding the example of methane, whose microbial production in soils is associated with large fractionations (Bréas *et al.*, 2001), soil emitted VOCs may constitute the source with the most uncertain signature. In case of CO, the aggregate of soil emissions is estimated to be negligibly small compared both to soil sink and overall CO

 turnover (Sanderson, 2002); even a radical change in its signature will be hardly reflected in the average $\delta^{13}C(CO)$.

[28] A somewhat similar case arises with the oceanic emissions for which the strengths are debatable, and no isotopic signa-tures were estimated for NMHCs. Rudolph (1997) suggests the photochemical processing of dissolved organic carbon (DOC) to be the origin of C in the ocean-emitted NMHCs. Within the current setup an *a priori* signature of −20.5‰ repre-senting the marine isotopic carbon content (Avery Jr *et al.*, 2006, lower limit) is assigned. This value is somewhat higher

 than −22‰ used for oceanic emissions by Stein and Rudolph (2007) in their modelling study on ethane isotopes. For CO, heavier oceanic emissions of −13.5‰ are assumed, according to Manning *et al.* (1997). This value is based on the inverse modelling study and observations in the SH, where ocean input on CO is evidently significant. Quite contrary to this value, Nakagawa *et al.* (2004) estimate the ocean emitted CO to possess a rather depleted composition of −40‰. This value ap-pears to be still questionable, as the composition of the seawater-extracted CO was measured, the assumed precursor DOC

 composition was depleted (of average −31‰) and the sampling was done in a single, fairly non-remote location in waters with high microbial activity (thus likely escorted with significant kinetic fractionation during the production). Finally, Bergamaschi *et al.* (2000) estimate the composition of CO emitted from the oceans to be as high as +5.1‰ (scenario S2). Similar to biofuel-related sources, the oceanic CO is associated with a very uncertain isotopic composition. The change of this source signature from −13.5‰ to −40‰ will result in the decrease of the average biogenic emission signature by 3‰

 with a corresponding 0.3‰ decrease in the overall CO surface emission composition.

3.3.1   Plant emissions

[29] For the plant biogenic emissions, a novel approach referring to the plant physiological properties is proposed here. In most previous (modelling) studies, the isotopic composition of the biogenically emitted tracers was based on the average global isotopic signature derived from the limited, often not consistent set of observations available. CO is a case in point

 here: The majority of the CO isotope modelling studies assume a $\delta^{13}C$ of CO emitted due the plant activity to be as low as −32.2‰, referring to the particular single estimate by Conny (1998). The latter was retrospectively derived from the obser-

vations at a rural US site (Stevens and Wagner, 1989), tolerating some important approximations, in particular (i) a two-component mixing model of the background and NMHC-only sources, (ii) constancy of the background composition throughout June to October, and (iii) neglecting the kinetic isotope fractionation caused by the CO sink. Whereas (i) is fairly applicable to the observations at a rural site, (ii) and (iii) rely on the five months constant background composition and neglect the variable input from the CO+OH reaction kinetic isotope effect (KIE). This is a too rough approximation, considering the intensive chemistry in the summer and characteristic CO lifetime shorter than a month. Indeed, the isotopic composition of background CO undergoes significant changes from spring to fall, and the competition of the CO+OH reaction KIE and the varying in-situ contribution from methane are the two non-negligible effects (Brenninkmeijer, 1993; Manning *et al.*, 1997; Röckmann *et al.*, 2002; Gromov *et al.*, 2010).

[30] Besides te temporal variation, the global average value does not represent the variable spatial distribution of the biogenic sources, which is important, since biogenic CO is mainly a product of the rapid oxidation of NMHCs. The latter, in turn, are expected to acquire specific isotopic ratios being emitted from various plant species under different environmental conditions. The most studied compound in this respect is isoprene (C_5H_8), one of the major biogenically released VOCs. Sharkey *et al.* (1991) measured the carbon isotopic composition of the emitted isoprene and found it dependent on the composition of the reservoir of recently fixed carbon (CO_2 incorporated in the plant material during the initial step of the photosynthetic cycle). The isotope effects related with the plant activity and plant-CO_2 exchanges are extensively studied (see, for instance, Dawson *et al.*, 2002). These usually operate with the isotope discrimination Δ, a representative parameter describing the fractionation of the plant tissue relative to the atmospheric reservoir (Farquhar *et al.*, 1989):

$$\Delta = \frac{\delta_a - \delta_p}{1 + \delta_p},$$ (11)

where δ_a and δ_p refer to the isotopic composition of the air CO_2 and plant tissues, respectively. In the form of Eq. (11), discrimination expresses the superposed effect of the various biological and plant physiological factors. The contribution of each of them, *e.g.* various plant metabolism pathways (C_3 or C_4, indices 3 and 4 indicate the number of carbons in the initial fixation product molecule), water availability (response to droughts), solar irradiance or various stress factors ought to be parameterised separately (Lloyd and Farquhar, 1994), which is a complex parameter. The largest effect on Δ is driven by the differences in the plant metabolism, the characteristic fixation mechanism of air CO_2 for the subsequent photosynthesis. The majority of the terrestrial plants incorporate the C_3 metabolism, when the fixation is escorted by the fractionation induced by RuBisCO (the specific enzyme used for the fixation in the so-called photosynthetic Calvin cycle). Accounting additionally for the other fractionations (*e.g.* diffusion of CO_2 through the stomata, *etc.*), typical Δ values for C_3 plants span from 15 ‰ to 25 ‰. Note that discrimination is expressed on the positive scale. Assuming a certain δ_a (approximately −8 ‰ for current air CO_2) and using Eq. (11), one derives the C_3 plant composition within the range of −32 ‰ to −23 ‰. C_4 plants employ other than RuBisCO enzymes; their efficiency is associated with lower Δ values of 2.5 ‰ to 5 ‰, corresponding to a −10 ‰ to −13 ‰ range of plant material $\delta^{13}C$. In addition to C_3 and C_4 plants, a minor fraction of terrestrial CAM (crassulacean acid

metabolism) plants exists. CAM can be regarded as a temporal coupling of C_3 and C_4 metabolisms employed by the plant for optimised adaptation to arid conditions. Therefore, CAM plants are characterised with the wide range of discriminations from 2‰ to 22‰ (Griffiths, 1992), or −10‰ to −30‰ expressed in $\delta^{13}C$ of the plant tissue carbon. The specified plant biomass compositions result from the permanent isotopic equilibration with the atmospheric pool (*i.e.* CO_2) accompanied by discrimination, thus the use of Eq. (11) is rational, when the long-term value of Δ is considered.

[31] In view of the correlation between the emitted species isotopic composition and the plant isotope discrimination, the latter is assumed here as a proxy for biogenic emission signatures in the current emission setup, rather than the global average signature. This approach, however, premises the following key assumptions:

– Few studies indicate that a moderate part (9 % to 28 %, Schnitzler *et al.*, 2004; Karl *et al.*, 2002) of the emitted isoprene may be issued from a separate carbon source of the plant. Its composition may differ from that expected from Δ, the photosynthetically fixed carbon. Moreover, neither the isotopic composition of the suggested alternative sources was deduced, nor the fractionations associated with their incorporation in the emission product. Affek and Yakir (2003) overcame this issue showing that the long-term value of Δ may be used as a proxy for the average bulk leaf biomass value, thus concluding the depletion of the emitted isoprene with respect to the latter. It is important to note that the contribution of alternative sources becomes larger as the plant is put under stress (*e.g.*, experiments of Schnitzler *et al.* (2004) were partly carried in CO_2-free air). For natural conditions, the proportion of the non-photosynthetically fixed carbon is likely to be smaller.

– The abovementioned studies have analysed exclusively isoprene and methanol; no comparable measurements were performed regarding the other species. Nevertheless, there are isotopic compositions of biogenically emitted NMHCs/VOCs reported relative to the plant bulk leaf composition (Rudolph *et al.*, 2003; Sharkey *et al.*, 1991; Conny and Currie, 1996), as well as few measurements of the plant-emitted VOCs whose $\delta^{13}C$ is found comparable to that of the expected bulk composition (Giebel *et al.*, 2010). Thus, it is practicable to derive the emission signatures from the measured depletions of the trace gas composition relative to that of the plant leaf. It is tolerable under the assumption that the latter is determined by the long-term value of Δ yielding from the specific plant metabolism and diffusion/equilibrium effects of the CO_2 photosynthetic fixation and respiration.

[32] For constructing the emission signatures, the estimated global distribution of the leaf discrimination is taken from Scholze *et al.* (2008). They use a dynamic global vegetation model extended with the terrestrial isotopic carbon module. The parameterisation of the leaf carbon discrimination is based on the framework developed by Lloyd and Farquhar (1994) neglecting poorly understood fractionations in several processes involved in the photorespiration. The vegetation dynamics model accounts for the plant and soil carbon reservoirs and a set of numerous parameters including the vegetation composition, its productivity, fire disturbance, water availability and land use schemes, as well as climate forcing (monthly temperature, precipitation and cloud cover fields). For the detailed model description, the reader is referred to Scholze *et al.* (2003) and the abovementioned references. The simulated leaf discrimination for the year 1995 from the ISOLUCP experiment (de-

picted in Fig. 5, left panel) is adopted here. The characteristic variability of the global leaf discrimination magnitude is on the order of decades, thus the data referring to 1995 is reckoned to be consistent for the studied year 2000. The bulk leaf composition δ_p is calculated straight from the isotope discrimination defined in Eq. (11), for which the isotopic composition of CO_2, namely δ_a, is required. For the period of 1997−2005 (corresponding biomass burning data in the current setup), the estimate of the surface CO_2 isotopic composition from the GLOBALVIEW project (GLOBALVIEW-CO2C13, 2009) is taken. These data comprise latitudinal weekly averages (shown in Fig. 5, right panel), and hence the latitudinal mean of the $\delta^{13}C(CO_2)$ went into the calculations. Except for isoprene and methanol, the fractionations accompanying the emissions are considered to be negligibly small, as no significant deviation (within measurement standard deviation of 1‰) from the source plant material for the selected NMHCs was reported (Conny and Currie, 1996; Guo et al., 2009). For the fractionation escorting isoprene emission, the lower limit of 4‰ depletion relative to the bulk leaf composition from Affek and Yakir (2003) is taken. In the case of methanol, significantly larger depletions (about 40‰) were discovered by Keppler et al., 2004 and linked to highly depleted pectin and lignin methoxyl pools which plants likely use to produce CH_3OH. A later work by Yamada et al. (2010) confirmed similar fractionations for a different set of C_3 plants species. Using the data from both studies, we reckon the depletion of (39±6.3)‰ w.r.t. the bulk composition of the plant for the emission of methanol from plants. Noteworthy, this value represents only two C_4 and one CAM plant species out of total 18 species regarded in these studies.

[33] The biogenic emission strengths and resulting isotopic signatures (average values for the year 2000) are listed in Table 4. The largest offline emissions pertain to CO and methanol. The final signatures reflect the proportion of the land (average −25.7‰) and oceanic sources, with an exception of much depleted methanol emission of −64.8‰ in $\delta^{13}C$. The average composition of the CO emission of −24.2‰ implies considerably lower ^{13}C depletion compared to the previously assumed −32.2‰ (Conny, 1998), which results in an effective increase of about +0.8‰ in the overall surface emission $\delta^{13}C$ value. The major part of the emissions is placed in the tropics, with the summer-triggered large emission in the NH. An example for CO is sketched in Fig. 6. The largest influx is associated with the areas of rather depleted sources. The land sources are comparable to the oceanic sources in NH winter, which is reflected in the zonal average $\delta^{13}C$ of CO emission. Based on the same proxy, the dynamics of the emission $\delta^{13}C$ value is similar for the other species.

[34] The isoprene emission, in turn, is calculated on-line, utilising model parameters obtained during the calculation. The emission parameterisation is described by Ganzeveld et al. (2002) and implemented for EMAC in the ONEMIS (formerly ONLEM) sub-model (Kerkweg et al., 2006). The key variables for the C_5H_8 emission are the temperature and radiative balance over the canopy (both are provided by the base model) and the vegetation foliar density (prescribed). The isoprene influx is calculated every model time step from the abovementioned variables. To account for the isotopic C_5H_8 emission, the necessary extension to ONEMIS was implemented. The influxes of the ^{12}C and ^{13}C isotopologues are calculated from the original isoprene emission flux and either simulated or prescribed average CO_2 isotopic composition. The leaf discrimination distribution is imported as a parameter (similar to the other prescribed data fields). The overall C_5H_8 emission ranges within 350−380 Tg yr^{-1} with the corresponding average ^{13}C signature within the range of −28.6‰ to −27.2‰ depending on sea-

sonal and spatial emission flux variation. As indirect (in-situ oxidation) source of CO, isoprene dominates over the sum of all remaining VOCs accounted for in the setup.

3.4 Final composition of the surface sources

[35] Table 5 lists the annually integrated trace gas emissions from the surface in the reference emission setup of this study. For the carbonaceous species, stable carbon isotopic compositions resulting from the superposition of the various emission types are given; values refer to the year 2000. The inter-annual variation for 1997−2005 of the average δ^{13}C signature of emitted CO is less than $0.5\,\text{‰}\,\text{yr}^{-1}$ resulting from the variability of $\pm 0.6\,\text{‰}\,\text{yr}^{-1}$ in the biomass-burned carbon and a negative trend in the CO_2 composition in the last decades ($-0.02\,\text{‰}$ to $-0.03\,\text{‰}\,\text{yr}^{-1}$ due to the input of fossil fuel-derived carbon into the atmosphere, Yakir, 2011) propagating into the biogenic emissions.

[36] The spatial distribution and annual dynamics of the surface CO emission is presented in Fig. 7. The largest emission is situated in the tropics, particularly in Africa and Asia and attributed to the biomass burning season in July-September in the SH, African fires in December and high-latitude fires in Eurasia and Northern America from May to September. A substantial proportion made up by the anthropogenic sources has no distinct seasonality and is prominent in the NH high latitudes; these are mostly transportation and industry (*i.e.*, fossil fuel related) sources. The relative dynamics of the isotopic composition is weaker than that of the corresponding flux magnitudes, indicating that the dominant sources are close to the average $-25\,\text{‰}$ to $-27\,\text{‰}$ of terrestrial carbon, with the exception of the North African and Australian fires, when a significant proportion of C_4 plants is being burnt. The largest portion of ^{13}C-enriched CO enters the atmosphere from December to March from the African equatorial fires. Interestingly, mixing of the fossil fuel-derived CO from ships and the heavier oceanic CO emissions highlights the most navigated ship tracks in the δ^{13}C(CO) map, where the strengths of these sources become comparable.

[37] The average compositions of the majority of NMHCs/VOCs fall in the range of $-26\,\text{‰}$ to $-24\,\text{‰}$ with the exception of isoprene, methanol, propane and butane (Fig. 8). For the latter two, the emission is coming predominantly from anthropogenic sources, which are close to $-27\,\text{‰}$. The isoprene and methanol composition reflect the significant depletion from the average terrestrial carbon composition. The annual emission dynamics for NMHCs/VOCs generally follows the proportion of the sources, *e.g.* variations for CH_3OH and CH_3COCH_3 are mainly driven by seasonality in biogenic emission. The source dynamics for various NMHCs/VOCs resemble each other being derived from the same proxies (*e.g.* burnt carbon in GFED). The uncertainties associated with emission fluxes and corresponding isotope signatures are discussed below in Sect. 3.6.

3.5 Pseudo-emission data

[38] For the few long-lived tracers in the current setup the pseudo-emission approach is applied by performing the relaxation of the selected species mixing ratios towards the lower boundary conditions (see also Sect. 2 above). The relaxation is handled by the TNUDGE submodel (Kerkweg *et al.*, 2006) and applied at every model time step with typical relaxation times of

3 h for the less reactive compounds (*e.g.* CH_4, CO_2, N_2O, *etc.*) . The nudging fields are based on the observed mixing ratios from the AGAGE database (Prinn *et al.*, 2000). Amongst the tracers undergoing nudging, CH_4, CH_3CCl_3, CCl_4, CH_3Cl, and CO_2 are isotopically separated. For CO_2, the time series of the zonally averaged composition from the GLOBALVIEW-CO2C13 database (described above in Sect. 3.3.1, see also Fig. 5) was superimposed on the regular CO_2 nudging fields from the EVAL$_2$ setup.

[39] Methane (CH_4) is the major atmospheric in-situ source of CO and other reactive carbonaceous species participating in the $CH_4 \rightarrow CO$ oxidation chain. Tropospheric CH_4 possesses a markedly ^{13}C-depleted composition, particularly due to the large contribution of the sources associated with the biogenic activity that produces isotopically light methane (see Bréas *et al.*, 2001 and references therein). The average tropospheric $\delta^{13}C(CH_4)$ value of $-47.3\,‰$ (corresponding to the year 2000) ensues from the composition of the surface sources (estimated equilibrated average of $-51.2\,‰$) and atmospheric oxidation KIEs, of which the reaction with OH ($+3.9\,‰$) is the dominant in the troposphere (Saueressig *et al.*, 2001). Since methane is largely abundant and long-lived, its signature shows a low variability on top of a weak long term trend (about $+0.3\,‰$ per decade around the year 2000, Lassey *et al.*, 2000) due to the input of the industrial fossil carbon, and little spatial and temporal variability. Quay *et al.* (1999) estimated the hemispheric gradient (averages of $-47.2\,‰$ *vs.* $-47.4\,‰$ for the SH and NH, respectively) and the monthly variation of $\delta^{13}C(CH_4)$ to be both on the order of $\pm0.2\,‰$. That is negligible in view of $\pm3\,‰$ variations in tropospheric δ^{13}C of CO and its large surface sources. Therefore, the constant value of $-47.2\,‰$ is applied to isotopically separate the original nudging fields of CH_4 in the current setup.

[40] Among the chlorinated hydrocarbons, the only in-situ source of C accounted for in the employed chemical mechanism of MECCA (as of EVAL$_2$ setup) is the photolysis of chloromethane yielding CH_3O_2. The remaining chlorinated hydrocarbons contribute only as the in-situ sources of Cl, thus their composition is omitted here. The main sources of chloromethane in the atmosphere are to date not clearly identified (Keppler *et al.*, 2005), the estimate of the average global isotopic atmospheric composition is $\delta^{13}C(CH_3Cl) = -32.6\,‰$ (Thompson *et al.*, 2002). This value is used for the pseudo-emission of chloromethane. The contribution of this source to the carbon pool in the atmosphere is low. The estimates of the primary CH_3Cl sink through the reaction with OH give a global average of 3.37 Tg(CH_3Cl) yr^{-1} equivalent to 0.8 Tg(C) yr^{-1} in the oxidised products (methyl peroxy radical).

3.6 Uncertainties

[41] In order to calculate the overall emission uncertainties in this study, we account for uncertainties associated with every emission source and its isotope signature, following the methodology described above (Sect. 2.2). The emission magnitudes and uncertainties are expressed in equivalent carbon units to avoid improper counting when isotope ratios are considered. Table 6 lists the uncertainties associated with every emission category/sector. For the fluxes, the so-called uncertainty factors (UF) are quoted, which are commonly reported in emission estimates and refer to a given confidence interval (CI) of emission flux (or typically underlying emission factor) with a given uncertainty probability density distribution (UPDD). For ex-

ample, the UF of 1.5 may imply that the 95 % CI of uncertainty spans from $F/1.5$ to $1.5 \cdot F$, or, in percent, from about $-33 \% \, F$ to $+50 \% \, F$, describing a log-normal UPDD around the median value of F. Exceptionally, the UFs reported for the EDGAR inventory (see Olivier *et al.*, 1999, Table 8) indicate the equivalent span (*i.e.*, Gaussian or any symmetric UPDD) range derived from the largest (*i.e.* upper end) value, that is for the above example would be $\pm 50 \% \, F$ around F. Such treatment is used in our analysis here (including reporting with the "±" notation) too, that is, selecting the largest (forward) uncertainty $\langle F \rangle$ using the relation

$$\frac{\langle F \rangle}{F} = (u_F - 1),\qquad(12)$$

where u_F is the uncertainty factor. In contrast, uncertainties of isotope signatures are reported plainly in ‰ of δ-values assuming normal (Gaussian) UPDD, as the isotopic ratios do not depend on the flux magnitudes.

[42] The uncertainties for some of the signatures have to be derived additionally, referring to the assumptions they are based on. Thus, the uncertainty of the $\delta^{13}C$ value of C_3 and C_4 plant material composites (*i.e.*, biofuel and biomass burning sources) is derived using Eq. (8) with the F_s and ^iR_s components substituted by the respective plant material fractions and $\delta^{13}C$ signatures. The uncertainties of the latter are inferred as two standard deviations of the signature distributions (assumed normal) based on the histogram data of the measured terrestrial compositions (Cerling *et al.*, 1999; Tipple and Pagani, 2007). The isotopic composition variability in C_3 plants is much larger than that of C_4, which is reflected in the resulting uncertainties of $\langle \delta^{13}C(C_3) \rangle = 5.7\,‰$ and $\langle \delta^{13}C(C_4) \rangle = 2.5\,‰$, respectively. This means that if, for instance, the plant is considered to be of the C_3 kind, its composition is likely to be found within the range of $\delta^{13}C(C_3) = -(27 \pm 2.9)\,‰$. From the "assumption" point of view, this uncertainty defines the degree of error introduced by prescribing all C_3 plants to have the composition of the distribution mode of $-27\,‰$. The errors associated with the plant compositions are the largest in this setup and they propagate to the final uncertainty mainly via the biofuel category. Interestingly, if one assumes that biofuel plant material comes predominantly from C_4 plants (*e.g.*, ethanol or biodiesel, see Sect. 3.2), it significantly decreases the overall uncertainty estimate.

[43] An additional calculation is required for those biogenic emissions originating from plants, whose signatures are derived from the leaf discrimination Δ and air CO_2 composition (see Eq. (11)). The uncertainty of the latter is on the order of $0.01\,‰$ according to the GLOBALVIEW-CO2C13 dataset (see http://www.esrl.noaa.gov/gmd/ccgg/globalview/gv_integration.html and references therein; here twice that value is assumed). The errors in Δ are as large as $2\,‰$, taking one standard deviation of the comparison of the simulated and measured characteristic discriminations for various plant functional types (Scholze *et al.*, 2008). The resulting propagated uncertainty amounts to $\langle \delta_p \rangle = 1.9\,‰$ (at the average global discrimination of $\Delta = 17\,‰$ and $\delta^{13}C(CO_2) = -8\,‰$) and accounts for all plant emissions, whose UFs of the magnitude of 3 are the largest (Guenther *et al.*, 1995). The uncertainty of the biomass burning signatures is set to $2\,‰$ referring to the upper limit of errors in atmospheric $\delta^{13}C$ used to validate the C_3/C_4 burnt vegetation distribution incorporated in the GFED v2.1 inventory (Still *et al.*, 2003). The UFs for biomass burning emissions are derived from the uncertainties on the estimates for global CO and carbon

release in fires by Arellano *et al.* (2006) for the April 2000 to March 2001 period obtained using the GFED data (van der Werf *et al.*, 2006).

[44] Employing the methodology described in Sect. 2.2, we derive the resulting overall (combined) uncertainties (listed in Table 5). Essentially high uncertainties are associated with isoprene and plant-dominated emissions of methanol (CH_3OH), acetone (CH_3COCH_3), dimethyl sulphide (DMS) and formic acid (HCOOH). The errors are lower (UFs of 1.5−2) for the species predominantly emitted from the fossil anthropogenic sources. Final uncertainties associated with the isotopic signatures are typically around 1‰, with the biofuel source having a large contribution of (0.3−0.4)‰. The terrestrial emissions are least uncertain resulting from the lower error in leaf carbon discrimination compared to the uncertainties from C_3/C_4 plant composites.

[45] Despite the large share of the biofuel sector emissions, the uncertainty of the CO $\delta^{13}C$ signature is 0.7‰ due to the compensating input from the fossil fuel sector with a signature of a higher certainty (0.3‰). The final emission strength is defined within ±17%, yet a rather large value. Reckoning the surface sources of about 1100 Tg yr^{-1} in the global turnover of CO of above 2600 Tg yr^{-1} (see the estimates in the following section), the emission uncertainties are expected to propagate in the model result errors with at most ±30% in CO mixing ratios and ±1.3‰ in $\delta^{13}C(CO)$, respectively. To estimate the uncertainties associated with the in-situ produced CO, the emission/isotope signature uncertainties of the respective NMHC/VOC sources should be used as the proxies accordingly.

4 Discussion

4.1 $^{13}CO/^{12}CO$ emissions

[46] Table 7 lists our resulting $^{13}C/^{12}C$-resolved CO emission inventory compared with the estimates available from previous studies. Notably, the bottom-up estimates (including the *a priori* setups for the inverse modelling studies) integrate more ^{13}C-depleted fluxes and vary less significantly between different studies, *i.e.* within −35‰ to −33‰ in $\delta^{13}C$. The earliest top-down estimate of −30.3‰ given by Stevens and Wagner (1989) (hereinafter denoted "SW89") is rather uncertain about the individual sources apportioning, being derived using the average atmospheric $\delta^{13}C(CO)$ observed by that time corrected for the average tropospheric ^{13}CO enrichment (reckoned to be +3‰ due to the KIE escorting CO removal by OH). Similar to SW89, the *a posteriori* estimates from the more elaborate inverse modelling studies favour the overall CO source $\delta^{13}C$ of −31.1‰ to −30.5‰ resulting from the larger ^{13}C-enriched surface influx and reduced methane oxidation source shares. The difference between the bottom-up and top-down estimates of the primary sources is 3−4‰, which, if one assumes the CO yield from CH_4 oxidation being nearly unity, causes an even larger disparity in the estimates of the average $\delta^{13}C$ of the non-CH_4 CO sources. Thus, from Manning *et al.* (1997) ("M97") and Bergamaschi *et al.* (2000) ("B00") these should be −21.3‰, whereas for the other studies the non-methane CO source signature is much lower, *e.g.* −26.1‰ in Emmons *et al.* (2004) ("E04") and −25.2‰ (this study, EVAL$_2$). From the CO budget considerations of Brenninkmeijer *et al.* (1999)

620 ("B99") one derives similarly ^{13}C-depleted source composition, when superimposing the respective $\delta^{13}C$ values from the literature on their reported emission strengths.

[47] Fig. 9 (right panel) details the global CO source by category from the previous and current isotope-enabled studies. Neither bottom-up nor top-down estimates show correlated tendencies, suggesting the overall CO budget being uncertain within at least ± 200 Tg(CO) yr^{-1}. One infers a similar estimate of about 2700 ± 280 Tg(CO) yr^{-1} from the results of the ensemble of

625 the inverse modelling approaches summarised by Duncan *et al.* (2007), narrowed down to 2500 ± 185 Tg(CO) yr^{-1} for the year 2000 (see refs. therein; quoted is the ensemble average ± 1 standard deviation, respectively). The large variation of $2500 - 2900$ Tg(CO) yr^{-1} of these estimates (quoted range refers to the year 2000 or to the interannual averages conferred by the studies regarded) is generally attributed to the differences in the implementation of inverted surface emission strengths. Regarding the variation range of individual CO sources between the studies, the largest spread of around 280 Tg(CO) yr^{-1} (or

630 equivalent 50 % of its average value) is attributed to the biomass burning (BB) source. The most ambiguous biogenic source (including oceanic emission) is varying within around 70 % of its average, or 90 Tg(CO) yr^{-1}, but is nonetheless least influential in the aggregate emission composition. The moderately uncertain fossil fuel/biofuel (FF/BF) and VOCs oxidation sources range within about 25 % and 30 % (170 and 150 Tg(CO) yr^{-1}), respectively. Disregarding the rather low *a posteriori* estimates of M97 and B00, the methane source of CO appears the most certain one ranging only within 15 %, or roughly

635 110 Tg(CO) yr^{-1} around its average value.

[48] Amongst the studies regarded here, the *a priori* and bottom up derived sources sum up to about 2900 Tg(CO) yr^{-1}, *i.e.* lie at the upper end of the range quoted above. The *a posteriori* sources in B00 are generally reduced at the expense of the smaller CH_4 source. In contrast to it, M97 compensate the decrease in the total photochemically produced CO by surface sources, thus keeping the final emission strengths close to the initial guess. Noteworthy, these two studies also infer the larg-

640 est BB emission sources exceeding the inter-study average by a factor of $^2/_3$ and $^1/_3$, respectively. A significantly lower CO budget in M97 is most probably the drawback of using the fairly limited observational data from the extratropical SH, where the inversion results are less sensitive to the NH sources, including their underestimation. Comparably low CO emissions for EMAC are derived here, which, when applied, are likely to result in systematically low simulated NH high-latitude CO mixing ratios, particularly in winter. A similar feature was observed in the previous studies with EMAC (Pozzer *et al.*, 2007,

645 their setup is being closely followed here, see Sect. 2), as well as in other models/inventories employed (*e.g.*, B00 and E04, see also Stein *et al.*, 2014, and refs. therein). Stein *et al.* (2014) show that a more detailed representation of the strength and seasonality of CO dry deposition fluxes and traffic emissions in Europe and North America leads to more adequately reproduced NH CO mixing ratios. Noteworthy, their hypothesis that the missing traffic CO is due to emission inventories not accounting for cold-start engine conditions should be verifiable through $^{18}O/^{16}O$ ratio of emitted CO: The latter (but unfortu-

650 nately not $^{13}C/^{12}C$ ratio) differ substantially between the BB and FF sources (see Kato *et al.* (1999a), also Sect. 3.1). Never-

theless, it is clear that strengths and spatial distribution of the missing CO sources shall receive a more thorough quantification through the isotope-resolved inventories, which we undertake in subsequent studies.

[49] In addition to the comparison of the CO source strengths, the left panel in Fig. 9 elucidates individual contributions of every source term to the δ^{13}C value of total emitted CO in the isotope-inclusive budget. The source terms (bars) are calculated as the products ($f_s \cdot \delta_s$), where f_s is the fractional contribution and δ_s is the δ^{13}C of a particular CO source, respectively. This way one grasps the integration of individual inputs enriching/depleting the final composition (with respect to the reference ratio of 0‰), which also highlights the inter-study variation of each source input. Because the majority of the CO sources is depleted, the calculated contributions are always negative, with an exception of the minute term of +0.1‰ in B00 from the oceanic source with a corresponding δ_s = +5.1‰ (added up to the biogenic category). Due to the appreciably ^{13}C-depleted composition of methane (−51.2‰), the overall composition is highly sensitive to the CH$_4$ source input, with clearly smaller contributions in M97 and B00. In contrast, the variation in the total surface source input to δ^{13}C is rather low, as opposed to the variation in respective fluxes.

[50] Coherent adjustments to the source composition in the *a posteriori* estimates are given by the inverse studies, however they remain within the uncertainty ranges of the *a priori* guesses (note that these are based on different isotope signatures as well, not listed in Table 7). Despite the improved uncertainties for almost each individual source category, the combined (either surface or total) *a posteriori* source estimates' uncertainties are essentially larger than those of the prior guesses, owing to the correlated nature of the inverted components (see Sect. 2.2 for elucidation). Thus, posterior combined uncertainties increase by a factor of 1.3−1.7 (fluxes) and 2.4−3.1 (flux δ^{13}C values) with respect to those of the independent priors, respectively. An exception is the reduction of uncertainty in the overall surface CO flux (factor 0.8) but not of its δ^{13}C value (increase, factor 1.2) in B00, which, however, does not reduce the final overall uncertainty.

[51] Furthermore, on a global scale the posterior repartitioning of the non-methane sources is virtually ineffective in M97: An increase of +2.7‰ in δ_s of the VOC oxidation source counterbalances the sufficiently larger BB source in the optimised emissions, hence the increase in tropospheric δ^{13}C(CO) is merely promoted by adjusting the CH$_4$ source. The reduction of the methane component in B00 is less marginal, whilst the non-methane sources also deplete the final δ^{13}C(CO) less, being enriched by a similar adjustment of the VOC signature by +2.5‰. Despite the fact that the CH$_4$ source strength inferred by B00 is comparable to the majority of the estimates presented in Fig. 9 (right panel), its relative contribution to the overall CO is diminished by a larger fraction of the other sources, which is a direct consequence of the reduced CO yield (0.86) from CH$_4$. The remaining studies suggest almost complete conversion of the CH$_4$+OH source to CO, and by this confine the overall source δ^{13}C to the −35‰ to −33‰ range. The results of the inversion studies (including the top-down estimate of SW89) importantly retain the *expected* tropospheric average of above −28‰ "assimilated" to a considerable extent from the observational data at the surface. Regarding the bottom-up estimates, it becomes clear that the CO+OH sink fractionation, when assumed to be about +3‰, is capable of bringing the tropospheric δ^{13}C(CO) value at most to −30.5‰, that is a perceptibly underestimated ^{13}CO/^{12}CO tropospheric ratio.

4.2 ^{13}C/^{12}C ratios of NMHCs/VOCs emission

[52] Only one ^{13}C-inclusive global-scale emission estimate for ethane is available to date for comparison with the NMHC/VOC emissions derived here. Using two 3D chemical transport models (CTM), Stein and Rudolph (2007) (hereinafter "SR07") evaluate two emission sets based on the GEIA/EDGAR inventories (detailed in Sect. 2), which differ in inclusion of the biofuel, biogenic and oceanic sources. Integrating the same literature sources (listed in Sect. 3), the authors use slightly different assumptions on the isotope composition of emitted C_2H_6, namely δ^{13}C signatures of C_4 plant carbon of −13‰, fossil-fuel carbon of −26‰ and gas production and transmission of −32‰, respectively. Furthermore, anthropogenic emission fluxes in SR07 are based on the previous version (2.0) of the EDGAR inventory. Being optimised in simulations with CTMs, emissions in SR07 offer more independent comparison against the current results based on the newer version (3.2) of EDGAR (see Sect. 3.1).

[53] Both estimates of C_2H_6 emission fluxes by SR07 are lower than, but within the uncertainty range of, the estimate reckoned here, *i.e.* 8.2 in MOZART CTM emissions ("MOZ") and 9.57 in GISS CTM emissions ("GISS") compared to 12.48±5.49 Tg(C_2H_2) yr^{-1} in EMAC, respectively. The δ^{13}C of total emitted ethane (−28.5‰) in MOZ is virtually identical to the value derived here (see Table 5), however it is composed of very different relative inputs (that is, the $f_s \cdot \delta_s$ terms, see previous section). Their shares (FF+BF : BB : biogenic) are lighter in the anthropogenic component in MOZ (−13.8‰ : −9.6‰ : −2.4‰) *vs.* that in EMAC (−19.6‰ : −5.3‰ : −0.9‰, respectively). Projecting the δ^{13}C signatures of MOZ onto the GISS fluxes yields slightly lower overall emission δ^{13}C of −26.6‰ (−19.8‰ : −6.8‰ : n/a), which is still on the lower end of −(25.9±0.8‰) obtained in EMAC. A similar projection of the emission δ^{13}C signatures used by SR07 onto the emission fluxes in EMAC, and *vice versa*, yields the large span of the overall emission δ^{13}C value of −(18.6−22.4)‰, which suggests that the ^{13}C-resolved C_2H_6 emission inventories should be rather sensitive to the ratio of anthropogenic and biogenic inputs. In this respect, the results obtained here for EMAC reconcile both the underestimated anthropogenic sources highlighted by SR07 and their (top-down) estimate of the global ethane δ^{13}C signature.

[54] SR07 do not provide a detailed uncertainty analysis for their emission estimates. Nonetheless, we attempt to derive these by applying the analysis and uncertainty factors reckoned for EMAC here (see Sect. 3.6, also Table 6), since similar emission categories and same literature sources are used. Thus derived global emission flux uncertainties in SR07 are of ±29% and ±32% in MOZ and GISS, respectively, and are noticeably lower than ±44% in EMAC, mostly owing to the different treatment of the BF sources (these are assumed by SR07 known with greater certainty, *i.e.* that of the FF sources). In contrast, the overall δ^{13}C signature uncertainties are only slightly improved w.r.t. to that in EMAC, *viz.* to ±0.7‰ and ±0.6‰ in MOZ and GISS, respectively. We therefore may conclude that all three estimates considered here agree in strength and isotope ratio of the global ethane emission flux.

5 Concluding remarks

[55] In this study, we attempt to deliver a comprehensive to date review on the ^{13}C/^{12}C ratios of emission sources of atmospheric CO and other reactive carbonaceous compounds. As a consistent starting point for the isotope extension, we choose the evaluated emission setup of the EMAC model (EVAL$_2$, see Sect. 2). The latter does not employ the most recent versions of some inventories (*e.g.*, EDGAR), however, we believe the information on proxies and the uncertainty analysis offered here should suffice and enable one to perform a complete isotope extension of any desired up-to-date inventory in a fashion similar to that presented here.

[56] Compiling the isotope-inclusive emission inventory immediately highlights several peculiarities of the ^{13}CO budget in comparison with previous studies:

– First, we corroborate that the bottom-up and top-down estimates disagree on the overall surface-emitted CO isotope signature, with the top down approaches reckoning it to be $(2-3)$‰ heavier in δ^{13}C. This discrepancy is larger than the associated uncertainties in all studies regarded here (an exception is the *a posteriori* estimate of M97) and calls further for clarification.

– Second, we note that our estimate has a substantially lower uncertainty (±0.7‰) associated with the total surface emission term. Furthermore, accurate use of probabilistic calculus renders the inverse modelling studies delivering *a posteriori* global estimates that are generally less certain (in case of correlated estimates) than their *a priori* guesses. This may leave bottom-up approaches favourable, as an increase in boundary condition data fed into inverse models does not necessarily reduce posterior uncertainties to adequate levels (*cf.* uncertainties in M97 and B00 with the latter utilising a substantially larger set of observational data).

– Third, isotope mass-balancing of the CO sources is very sensitive to the input of ^{13}C-depleted carbon from the CH$_4$ oxidation source (*cf.* Fig. 9 and Table 7), with the key question being the tropospheric yield of CO from methane oxidation. Although minor compared to the latter, production of CO from significantly ^{13}C-depleted methanol may aggravate this issue. Only E04 have explicitly accounted for CH$_3$OH in their model setup with average emission δ^{13}C of -30‰ compared to $-(61.4\pm3.6)$‰ in the curret setup with EMAC.

[57] The aspects outlined above highlight disagreements between the bottom-up and top-down approaches on ^{13}CO atmospheric budget, which are not reconciled yet. Perhaps, a hybrid iterative approach consisting of inverse modelling steps (performing optimisation of the emission fluxes only), followed by forward modelling steps (applying less uncertain bottom-up isotope signatures), could offer an efficient solution to this problem.

[58] At last, the comparison of our results with the study by SR07 on isotope-resolved ethane emissions evidences that isotope ratio information may bring deeper insight into studies dealing with NMHCs/VOCs as well, even at the stage of compiling the emission inventories, *e.g.* comparing their versions. We therefore hope that current results will bolster the community for further efforts in this yet little explored area of atmospheric isotope composition modelling field.

Acknowledgements. Authors are grateful to Alan Goldstein (UC Berkeley), Elena Popa (IMAU Utrecht) and Taku Umezawa (NIES Tsukuba) for fruitful discussions on CO and trace gas emissions and their isotope composition particularities. Andrea Pozzer (MPI-C Mainz) is acknowledged for the great help with the biogenic emissions in EMAC. We appreciate the expertise on standard isotope ratios application from Sergey Assonov (IAEA Environmental Labs Vienna), the erroneous formulation pointed out by Franziska Frank (DLR Oberpfaffenhofen) and important comments on the CH_3Cl isotope composition by Frank Keppler (GEOW Heidelberg). Last but not least, we are indebted to Astrid Kiendler-Scharr and two anonymous Referees whose expertise and valuable input led to substantial improvement of this manuscript.

Appendix

[59] We note that the value of $^{13}C R_{st}$ from (Craig (1957)) we use is nominally outdated since the last re-determination of the carbon isotope ratio of the NBS 19 reference material used to define the "hypothetical" V-PDB scale introduced after the former PDB primary material was exhausted (see Chapter 40 in de Groot, 2004, Zhang *et al.*, 1990 and Brand *et al.*, 2010). Owing to the differences between the former (*i.e.*, assigned from PDB) and revised scales, a change in isotope composition corresponding to 1 ‰ in $\delta^{13}C$ on the PDB-scale is about 0.001176 ‰ larger on the V-PDB scale, which implies *ex post facto* different absolute abundances derived using the same $\delta^{13}C$ values reported. The resulting emission $\delta^{13}C$ signatures presented here are sensitive to the choice of these standards, since absolute emission fluxes are defined through them. Nonetheless, errors introduced by adopting outdated values are negligible compared to uncertainties introduced by the other factors, *e.g.* laboratory/model estimates of the emission strengths and signatures (*cf.* Sect. 3.6, also Table 6).

References

Affek, H. P. and Yakir, D.: Natural Abundance Carbon Isotope Composition of Isoprene Reflects Incomplete Coupling between Isoprene Synthesis and Photosynthetic Carbon Flow, *Plant Physiol.*, **131**, 1727−1736, doi: 10.1104/pp.102.012294, 2003.

Andreae, M. O. and Merlet, P.: Emission of trace gases and aerosols from biomass burning, *Glob. Biogeochem. Cyc.*, **15**, 955−966, doi: 10.1029/2000gb001382, 2001.

Arellano, A. F., Jr., Kasibhatla, P. S., Giglio, L., van der Werf, G. R., Randerson, J. T., and Collatz, G. J.: Time-dependent inversion estimates of global biomass-burning CO emissions using Measurement of Pollution in the Troposphere (MOPITT) measurements, *J. Geophys. Res. Atm.*, **111**, D09303, doi: 10.1029/2005jd006613, 2006.

Avery Jr, G. B., Willey, J. D., and Kieber, R. J.: Carbon isotopic characterization of dissolved organic carbon in rainwater: Terrestrial and marine influences, *Atmos. Environ.*, **40**, 7539−7545, doi: 10.1016/j.atmosenv.2006.07.014, 2006.

Bates, T. S., Kelly, K. C., Johnson, J. E., and Gammon, R. H.: Regional and seasonal variations in the flux of oceanic carbon monoxide to the atmosphere, *J. Geophys. Res. Atm.*, **100**, 23093−23101, doi: 10.1029/95jd02737, 1995.

Bergamaschi, P., Hein, R., Brenninkmeijer, C. A. M., and Crutzen, P. J.: Inverse modeling of the global CO cycle 2. Inversion of $^{13}C/^{12}C$ and $^{18}O/^{16}O$ isotope ratios, *J. Geophys. Res. Atm.*, **105**, 1929−1945, doi: 10.1029/1999jd900819, 2000.

Boutton, T. W.: Stable carbon isotope ratios of natural materials: II. Atmospheric, terrestrial, marine, and freshwater environments, in: Carbon Isotope Techniques, edited by: Coleman, D. and Fry, B., Elsevier, New York, 173−185, 1991.

Brand, W. A., Assonov, S. S., and Coplen, T. B.: Correction for the ^{17}O interference in $\delta^{13}C$ measurements when analyzing CO_2 with stable isotope mass spectrometry (IUPAC Technical Report), *Pure Appl. Chem.*, **82**, 1719−1733, doi: 10.1351/pac-rep-09-01-05, 2010.

Bréas, O., Guillou, C., Reniero, F., and Wada, E.: The global methane cycle: isotopes and mixing ratios, sources and sinks, *Isot. Env. Health Stud.*, **37**, 257−379, doi: 10.1080/10256010108033302, 2001.

Brenninkmeijer, C. A. M.: Measurement of the abundance of ^{14}CO in the atmosphere and the $^{13}C/^{12}C$ and $^{18}O/^{16}O$ ratio of atmospheric CO with applications in New Zealand and Antarctica, *J. Geophys. Res. Atm.*, **98**, 10595−10614, doi: 10.1029/93JD00587, 1993.

Brenninkmeijer, C. A. M., Röckmann, T., Bräunlich, M., Jöckel, P., and Bergamaschi, P.: Review of progress in isotope studies of atmospheric carbon monoxide, *Chemosphere Glob. Sci. Change*, **1**, 33−52, doi: 10.1016/S1465-9972(99)00018-5, 1999.

Brenninkmeijer, C. A. M., Janssen, C., Kaiser, J., Röckmann, T., Rhee, T. S., and Assonov, S. S.: Isotope effects in the chemistry of atmospheric trace compounds, *Chem. Rev.*, **103**, 5125−5161, doi: 10.1021/Cr020644k, 2003.

Cerling, T. E., Harris, J. M., and Leakey, M. G.: Browsing and Grazing in Elephants: The Isotope Record of Modern and Fossil Proboscideans, *Oecologia*, **120**, 364−374, doi: 10.1007/s004420050869, 1999.

Conny, J. M. and Currie, L. A.: The isotopic characterization of methane, non-methane hydrocarbons and formaldehyde in the troposphere, *Atmos. Environ.*, **30**, 621−638, doi: 10.1016/1352-2310(95)00305-3, 1996.

Conny, J. M.: The isotopic characterization of carbon monoxide in the troposphere, *Atmos. Environ.*, **32**, 2669−2683, doi: 10.1016/S1352-2310(97)00398-1, 1998.

Craig, H.: Isotopic standards for carbon and oxygen and correction factors for mass-spectrometric analysis of carbon dioxide, *Geochim. Cosmochim. Acta*, **12**, 133−149, doi: 10.1016/0016-7037(57)90024-8, 1957.

Criss, R. E.: Principles of Stable Isotope Distribution, Oxford University Press, 264 pp., 1999.

Czapiewski, K. V., Czuba, E., Huang, L., Ernst, D., Norman, A. L., Koppmann, R., and Rudolph, J.: Isotopic composition of non-methane hydrocarbons in emissions from biomass burning, *J. Atmos. Chem.*, **43**, 45−60, doi: 10.1023/a:1016105030624, 2002.

D'Agostini, G.: Asymmetric Uncertainties: Sources, Treatment and Potential Dangers, **arXiv:physics/0403086**, 2004.

Dawson, T. E., Mambelli, S., Plamboeck, A. H., Templer, P. H., and Tu, K. P.: Stable Isotopes in Plant Ecology, *Annu. Rev. Ecol. Syst.*, **33**, 507−559, doi: 10.2307/3069272, 2002.

de Groot, P. A.: Handbook of Stable Isotope Analytical Techniques, Elsevier, 1234 pp., 2004.

Demirbas, A.: Biofuels sources, biofuel policy, biofuel economy and global biofuel projections, *Energ. Convers. Manage.*, **49**, 2106−2116, doi: 10.1016/j.enconman.2008.02.020, 2008.

Demirbas, A.: Political, economic and environmental impacts of biofuels: A review, *Appl. Energ.*, **86**, S108−S117, doi: 10.1016/j.apenergy.2009.04.036, 2009.

Drosg, M.: Dealing with Uncertainties: A Guide to Error Analysis, Springer, 235 pp., 2009.

Dube, O. P.: Linking fire and climate: interactions with land use, vegetation, and soil, *Curr. Opin. Environ. Sustain.*, **1**, 161−169, doi: 10.1016/j.cosust.2009.10.008, 2009.

Duncan, B. N., Logan, J. A., Bey, I., Megretskaia, I. A., Yantosca, R. M., Novelli, P. C., Jones, N. B., and Rinsland, C. P.: Global budget of CO, 1988-1997: Source estimates and validation with a global model, *J. Geophys. Res. Atm.*, **112**, D22301, doi: 10.1029/2007jd008459, 2007.

Emmons, L. K., Hess, P., Lamarque, J. F., Orlando, J. J., Pétron, G., Mak, J., Randerson, J., and Granier, C.: Improving CO Emissions using $^{13}C/^{12}C$ Fractions in Observations and MOZART, *8th International Global Atmospheric Chemistry Conference (IGAC 2004)*, Christchurch, New Zealand, 2004.

Enting, I. G.: Inverse problems in atmospheric constituent transport, Cambridge University Press, 2002.

Farquhar, G. D., Ehleringer, J. R., and Hubick, K. T.: Carbon Isotope Discrimination and Photosynthesis, *Annu. Rev. Plant Phys. Molec. Biol.*, **40**, 503−537, doi: 10.1146/annurev.pp.40.060189.002443, 1989.

Ganzeveld, L. N., Lelieveld, J., Dentener, F. J., Krol, M. C., Bouwman, A. J., and Roelofs, G. J.: Global soil-biogenic NOx emissions and the role of canopy processes, *J. Geophys. Res. Atm.*, **107**, 4298, doi: 10.1029/2001jd001289, 2002.

Gensch, I., Kiendler-Scharr, A., and Rudolph, J.: Isotope ratio studies of atmospheric organic compounds: Principles, methods, applications and potential, *International Journal of Mass Spectrometry*, **365–366**, 206−221, doi: 10.1016/j.ijms.2014.02.004, 2014.

Giebel, B. M., Swart, P. K., and Riemer, D. D.: $\delta^{13}C$ Stable Isotope Analysis of Atmospheric Oxygenated Volatile Organic Compounds by Gas Chromatography-Isotope Ratio Mass Spectrometry, *Anal. Chem.*, **82**, 6797−6806, doi: 10.1021/ac1007442, 2010.

GLOBALVIEW-CO2C13: Cooperative Atmospheric Data Integration Project – δ¹³C of Carbon Dioxide, CD-ROM [Also available on Internet via anonymous FTP to ftp.cmdl.noaa.gov, Path: ccg/co2c13/GLOBALVIEW], NOAA ESRL, Boulder, Colorado, http://www.esrl.noaa.gov/gmd/ccgg/globalview/, 2009.

Goldstein, A. H. and Shaw, S. L.: Isotopes of Volatile Organic Compounds: An Emerging Approach for Studying Atmospheric Budgets and Chemistry, *Chem. Rev.*, **103**, 5025−5048, doi: 10.1021/cr0206566, 2003.

Griffiths, H.: Carbon isotope discrimination and the integration of carbon assimilation pathways in terrestrial CAM plants, *Plant Cell Environ.*, **15**, 1051−1062, doi: 10.1111/j.1365-3040.1992.tb01655.x, 1992.

Gromov, S., Jöckel, P., Sander, R., and Brenninkmeijer, C. A. M.: A kinetic chemistry tagging technique and its application to modelling the stable isotopic composition of atmospheric trace gases, *Geosci. Model Dev.*, **3**, 337−364, doi: 10.5194/gmd-3-337-2010, 2010.

Guenther, A., Hewitt, C. N., Erickson, D., Fall, R., Geron, C., Graedel, T., Harley, P., Klinger, L., Lerdau, M., McKay, W. A., Pierce, T., Scholes, B., Steinbrecher, R., Tallamraju, R., Taylor, J., and Zimmerman, P.: A global model of natural volatile organic compound emissions, *J. Geophys. Res. Atm.*, **100**, 8873−8892, doi: 10.1029/94jd02950, 1995.

Guo, S., Wen, S., Wang, X., Sheng, G., Fu, J., Hu, P., and Yu, Y.: Carbon isotope analysis for source identification of atmospheric formaldehyde and acetaldehyde in Dinghushan Biosphere Reserve in South China, *Atmos. Environ.*, **43**, 3489−3495, doi: 10.1016/j.atmosenv.2009.04.041, 2009.

Ho, K. F., Lee, S. C., Ho, W. K., Blake, D. R., Cheng, Y., Li, Y. S., Ho, S. S. H., Fung, K., Louie, P. K. K., and Park, D.: Vehicular emission of volatile organic compounds (VOCs) from a tunnel study in Hong Kong, *Atmos. Chem. Phys.*, **9**, 7491−7504, doi: 10.5194/acp-9-7491-2009, 2009.

IISI: Steel statistical yearbook 2003, International Iron and Steel Institute, Brussels, http://www.worldsteel.org/en/dam/jcr:c7c68146-a56c-4f33-bac9-68737f6c2242/Steel+statistical+yearbook+2003.pdf, 2004.

Jöckel, P., Sander, R., Kerkweg, A., Tost, H., and Lelieveld, J.: Technical note: The Modular Earth Submodel System (MESSy) – a new approach towards Earth System Modeling, *Atmos. Chem. Phys.*, **5**, 433−444, doi: 10.5194/acp-5-433-2005, 2005.

Jöckel, P.: Technical note: Recursive rediscretisation of geo-scientific data in the Modular Earth Submodel System (MESSy), *Atmos. Chem. Phys.*, **6**, 3557−3562, doi: 10.5194/acp-6-3557-2006, 2006.

Jöckel, P., Tost, H., Pozzer, A., Brühl, C., Buchholz, J., Ganzeveld, L., Hoor, P., Kerkweg, A., Lawrence, M. G., Sander, R., Steil, B., Stiller, G., Tanarhte, M., Taraborrelli, D., van Aardenne, J., and Lelieveld, J.: The atmospheric chemistry general circulation model ECHAM5/MESSy1: consistent simulation of ozone from the surface to the mesosphere, *Atmos. Chem. Phys.*, **6**, 5067−5104, doi: 10.5194/acp-6-5067-2006, 2006.

Jöckel, P., Kerkweg, A., Pozzer, A., Sander, R., Tost, H., Riede, H., Baumgaertner, A., Gromov, S., and Kern, B.: Development cycle 2 of the Modular Earth Submodel System (MESSy2), *Geosci. Model Dev.*, **3**, 717−752, doi: 10.5194/gmd-3-717-2010, 2010.

Johnke, B.: Emissions from waste incineration, IPCC NGGIP Publication, http://www.ipcc-nggip.iges.or.jp/public/gp/english/index.html, 2000.

Johnson, B. J. and Dawson, G. A.: A Preliminary Study of the Carbon-Isotopic Content of Ambient Formic Acid and Two Selected Sources: Automobile Exhaust and Formicine Ants, *J. Atmos. Chem.*, **17**, 123−140, doi: 10.1007/BF00702822, 1993.

Karl, T., Fall, R., Rosenstiel, T., Prazeller, P., Larsen, B., Seufert, G., and Lindinger, W.: On-line analysis of the ¹³CO₂ labeling of leaf isoprene suggests multiple subcellular origins of isoprene precursors, *Planta*, **215**, 894−905, doi: 10.1007/s00425-002-0825-2, 2002.

Kato, S., Akimoto, H., Bräunlich, M., Röckmann, T., and Brenninkmeijer, C. A. M.: Measurements of stable carbon and oxygen isotopic compositions of CO in automobile exhausts and ambient air from semi-urban Mainz, Germany, *Geochem. J.*, **33**, 73-77, doi: 10.2343/geochemj.33.73, 1999a.

Kato, S., Akimoto, H., Röckmann, T., Bräunlich, M., and Brenninkmeijer, C. A. M.: Stable isotopic compositions of carbon monoxide from biomass burning experiments, *Atmos. Environ.*, **33**, 4357−4362, doi: 10.1016/S1352-2310(99)00243-5, 1999b.

Keppler, F., Kalin, R. M., Harper, D. B., McRoberts, W. C., and Hamilton, J. T. G.: Carbon isotope anomaly in the major plant C₁ pool and its global biogeochemical implications, *Biogeosci.*, **1**, 123−131, doi: 10.5194/bg-1-123-2004, 2004.

Keppler, F., Harper, D. B., Röckmann, T., Moore, R. M., and Hamilton, J. T. G.: New insight into the atmospheric chloromethane budget gained using stable carbon isotope ratios, *Atmos. Chem. Phys.*, **5**, 2403−2411, doi: 10.5194/acp-5-2403-2005, 2005.

Kerkweg, A., Sander, R., Tost, H., and Jöckel, P.: Technical note: Implementation of prescribed (OFFLEM), calculated (ONLEM), and pseudo-emissions (TNUDGE) of chemical species in the Modular Earth Submodel System (MESSy), *Atmos. Chem. Phys.*, **6**, 3603−3609, doi: 10.5194/acp-6-3603-2006, 2006.

Kesselmeier, J. and Staudt, M.: Biogenic Volatile Organic Compounds (VOC): An Overview on Emission, Physiology and Ecology, *J. Atmos. Chem.*, **33**, 23−88, doi: 10.1023/a:1006127516791, 1999.

Komatsu, D. D., Tsunogai, U., Yamaguchi, J., and Nakagawa, F.: A selective unsaturated hydrocarbon subtraction technique for stable carbon isotopic analysis of atmospheric methyl chloride, methyl bromide, and C_2-C_5 saturated hydrocarbons using continuous-flow isotope ratio mass spectrometry, *Rapid Commun. Mass Spectrom.*, **19**, 477−483, doi: 10.1002/rcm.1795, 2005.

Lassey, K. R., Lowe, D. C., and Manning, M. R.: The trend in atmospheric methane $\delta^{13}C$ and implications for isotopic constraints on the global methane budget, *Glob. Biogeochem. Cyc.*, **14**, 41−49, doi: 10.1029/1999gb900094, 2000.

Lloyd, J. and Farquhar, G. D.: ^{13}C discrimination during CO_2 assimilation by the terrestrial biosphere, *Oecologia*, **99**, 201−215, doi: 10.1007/BF00627732, 1994.

Manning, M. R., Brenninkmeijer, C. A. M., and Allan, W.: Atmospheric carbon monoxide budget of the southern hemisphere: Implications of $^{13}C/^{12}C$ measurements, *J. Geophys. Res. Atm.*, **102**, 10673−10682, doi: 10.1029/96JD02743, 1997.

Nakagawa, F., Tsunogai, U., Gamo, T., and Yoshida, N.: Stable isotopic compositions and fractionations of carbon monoxide at coastal and open ocean stations in the Pacific, *J. Geopys. Res. Oceans*, **109**, C06016, doi: 10.1029/2001jc001108, 2004.

Nara, H., Nakagawa, F., and Yoshida, N.: Development of two-dimensional gas chromatography/isotope ratio mass spectrometry for the stable carbon isotopic analysis of C_2-C_5 non-methane hydrocarbons emitted from biomass burning, *Rapid Commun. Mass Spectrom.*, **20**, 241−247, doi: 10.1002/rcm.2302, 2006.

O'Connor, D.: GHG Emission Reductions From World Biofuel Production And Use, S&T Squared Consultants, Delta, BC Canada, V4E 2Z2, 2009.

Olivier, J. G. J., Bloos, J. P. J., Berdowski, J. J. M., Visschedijk, A. J. H., and Bouwman, A. F.: A 1990 global emission inventory of anthropogenic sources of carbon monoxide on 1°×1° developed in the framework of EDGAR/GEIA, *Chemosphere Glob. Sci. Change*, **1**, 1−17, doi: 10.1016/s1465-9972(99)00019-7, 1999.

Olivier, J. G. J., Berdowski, J. J. M., Peters, J. A. H. W., Bakker, J., Visschedijk, A. J. H., and Bloos, J. P. J.: Applications of EDGAR including a description of EDGAR 3.2: reference database with trend data for 1970−1995, National Institute for Public Health and the Environment (RIVM), 142, 2002.

Popa, M. E., Vollmer, M. K., Jordan, A., Brand, W. A., Pathirana, S. L., Rothe, M., and Röckmann, T.: Vehicle emissions of greenhouse gases and related tracers from a tunnel study: CO : CO_2, N_2O : CO_2, CH_4 : CO_2, O_2 : CO_2 ratios, and the stable isotopes ^{13}C and ^{18}O in CO_2 and CO, *Atmos. Chem. Phys.*, **14**, 2105-2123, doi: 10.5194/acp-14-2105-2014, 2014.

Pozzer, A., Jockel, P., Tost, H., Sander, R., Ganzeveld, L., Kerkweg, A., and Lelieveld, J.: Simulating organic species with the global atmospheric chemistry general circulation model ECHAM5/MESSy1: a comparison of model results with observations, *Atmos. Chem. Phys.*, **7**, 2527−2550, doi: 10.5194/acp-7-2527-2007, 2007.

Pozzer, A., Jockel, P., and van Aardenne, J.: The influence of the vertical distribution of emissions on tropospheric chemistry, *Atmos. Chem. Phys.*, **9**, 9417−9432, doi: 10.5194/acp-9-9417-2009, 2009.

Prinn, R. G., Weiss, R. F., Fraser, P. J., Simmonds, P. G., Cunnold, D. M., Alyea, F. N., O'Doherty, S., Salameh, P., Miller, B. R., Huang, J., Wang, R. H. J., Hartley, D. E., Harth, C., Steele, L. P., Sturrock, G., Midgley, P. M., and McCulloch, A.: A history of chemically and radiatively important gases in air deduced from ALE/GAGE/AGAGE, *J. Geophys. Res. Atm.*, **105**, 17751−17792, doi: 10.1029/2000jd900141, http://agage.eas.gatech.edu/, 2000.

Quay, P., Stutsman, J., Wilbur, D., Snover, A., Dlugokencky, E., and Brown, T.: The isotopic composition of atmospheric methane, *Glob. Biogeochem. Cyc.*, **13**, 445−461, doi: 10.1029/1998gb900006, 1999.

Randerson, J. T., van der Werf, G. R., Collatz, G. J., Giglio, L., Still, C. J., Kasibhatla, P., Miller, J. B., White, J. W. C., DeFries, R. S., and Kasischke, E. S.: Fire emissions from C_3 and C_4 vegetation and their influence on interannual variability of atmospheric CO_2 and $\delta^{13}CO_2$, *Glob. Biogeochem. Cyc.*, **19**, GB2019, doi: 10.1029/2004gb002366, 2005.

Randerson, J. T., van der Werf, G. R., Giglio, L., Collatz, G. J., and Kasibhatla, P. S.: Global Fire Emissions Database, Version 2 (GFED v2.1), Oak Ridge National Laboratory Distributed Active Archive Center, Oak Ridge, Tennessee, USA, http://daac.ornl.gov/, 2007.

Röckmann, T., Jöckel, P., Gros, V., Bräunlich, M., Possnert, G., and Brenninkmeijer, C. A. M.: Using ^{14}C, ^{13}C, ^{18}O and ^{17}O isotopic variations to provide insights into the high northern latitude surface CO inventory, *Atmos. Chem. Phys.*, **2**, 147−159, doi: 10.5194/acp-2-147-2002, 2002.

Rudolph, J.: Biogenic sources of atmospheric alkenes and acetylene, in: Biogenic Volatile Organic Compounds in the Atmosphere – Summary of Present Knowledge, edited by: Helas, G., Slanina, S., and R., S., SPB Academic Publishers, Amsterdam, The Netherlands, 53−65, 1997.

Rudolph, J., Czuba, E., Norman, A. L., Huang, L., and Ernst, D.: Stable carbon isotope composition of nonmethane hydrocarbons in emissions from transportation related sources and atmospheric observations in an urban atmosphere, *Atmos. Environ.*, **36**, 1173−1181, doi: 10.1016/S1352-2310(01)00537-4, 2002.

Rudolph, J., Anderson, R. S., Czapiewski, K. V., Czuba, E., Ernst, D., Gillespie, T., Huang, L., Rigby, C., and Thompson, A. E.: The Stable Carbon Isotope Ratio of Biogenic Emissions of Isoprene and the Potential Use of Stable Isotope Ratio Measurements to Study Photochemical Processing of Isoprene in the Atmosphere, *J. Atmos. Chem.*, **44**, 39−55, doi: 10.1023/a:1022116304550, 2003.

Sander, R., Baumgaertner, A., Gromov, S., Harder, H., Jöckel, P., Kerkweg, A., Kubistin, D., Regelin, E., Riede, H., Sandu, A., Taraborrelli, D., Tost, H., and Xie, Z. Q.: The atmospheric chemistry box model CAABA/MECCA-3.0, *Geosci. Model Dev.*, **4**, 373−380, doi: 10.5194/gmd-4-373-2011, 2011.

Sanderson, M. G.: Emission of Carbon Monoxide by Vegetation and Soils, https://library.metoffice.gov.uk/M10326UK/OPAC/Details/Record.aspx?BibCode=14947676, 2002.

Saueressig, G., Crowley, J. N., Bergamaschi, P., Brühl, C., Brenninkmeijer, C. A. M., and Fischer, H.: Carbon 13 and D kinetic isotope effects in the reactions of CH_4 with $O(^1D)$ and OH: New laboratory measurements and their implications for the isotopic composition of stratospheric methane, *J. Geophys. Res. Atm.*, **106**, 23127−23138, doi: 10.1029/2000jd000120, 2001.

Saurer, M., Prevot, A. S. H., Dommen, J., Sandradewi, J., Baltensperger, U., and Siegwolf, R. T. W.: The influence of traffic and wood combustion on the stable isotopic composition of carbon monoxide, *Atmos. Chem. Phys.*, **9**, 3147−3161, 2009.

Schmitt, A. and Brunner, B.: Emissions from aviation and their development over time, DLR-Mitteilung 97-04, 1−301, 1997.

Schnitzler, J.-P., Graus, M., Kreuzwieser, J., Heizmann, U., Rennenberg, H., Wisthaler, A., and Hansel, A.: Contribution of Different Carbon Sources to Isoprene Biosynthesis in Poplar Leaves, *Plant Physiol.*, **135**, 152−160, doi: 10.1104/pp.103.037374, 2004.

Scholze, M., Kaplan, J. O., Knorr, W., and Heimann, M.: Climate and interannual variability of the atmosphere-biosphere $^{13}CO_2$ flux, *Geophys. Res. Lett.*, **30**, 1097, doi: 10.1029/2002gl015631, 2003.

Scholze, M., Ciais, P., and Heimann, M.: Modeling terrestrial ^{13}C cycling: Climate, land use and fire, *Glob. Biogeochem. Cyc.*, **22**, GB1009, doi: 10.1029/2006gb002899, 2008.

Sharkey, T. D., Loreto, F., Delwiche, C. F., and Treichel, I. W.: Fractionation of Carbon Isotopes during Biogenesis of Atmospheric Isoprene, *Plant Physiol.*, **97**, 463−466, doi: 10.1104/pp.97.1.463, 1991.

Soja, A. J., Cofer, W. R., Shugart, H. H., Sukhinin, A. I., Stackhouse, P. W., Jr., McRae, D. J., and Conard, S. G.: Estimating fire emissions and disparities in boreal Siberia (1998–2002), *J. Geophys. Res. Atm.*, **109**, D14S06, doi: 10.1029/2004jd004570, 2004.

Stein, O. and Rudolph, J.: Modeling and interpretation of stable carbon isotope ratios of ethane in global chemical transport models, *J. Geophys. Res. Atm.*, **112**, D14308, doi: 10.1029/2006jd008062, 2007.

Stein, O., Schultz, M. G., Bouarar, I., Clark, H., Huijnen, V., Gaudel, A., George, M., and Clerbaux, C.: On the wintertime low bias of Northern Hemisphere carbon monoxide found in global model simulations, *Atmos. Chem. Phys.*, **14**, 9295−9316, doi: 10.5194/acp-14-9295-2014, 2014.

Stevens, C. M., Walling, D., Venters, A., Ross, L. E., Engelkemeir, A., and Krout, L.: Isotopic Composition of Atmospheric Carbon Monoxide, *Earth Planet. Sci. Lett.*, **16**, 147−165, doi: 10.1016/0012-821X(72)90183-5, 1972.

Stevens, C. M. and Wagner, A. F.: The Role of Isotope Fractionation Effects in Atmospheric Chemistry, *Z. Naturforsch. A*, **44a**, 376−384, 1989.

Still, C. J., Berry, J. A., Collatz, G. J., and DeFries, R. S.: Global distribution of C_3 and C_4 vegetation: Carbon cycle implications, *Glob. Biogeochem. Cyc.*, **17**, 1006, doi: 10.1029/2001gb001807, 2003.

Tarantola, A.: Inverse Problem Theory and Methods for Model Parameter Estimation, Other Titles in Applied Mathematics, Society for Industrial and Applied Mathematics, 342 pp., 2005.

Thompson, A., Anderson, R., Rudolph, J., and Huang, L.: Stable carbon isotope signatures of background tropospheric chloromethane and CFC113, *Biogeochemistry*, **60**, 191−211, doi: 10.1023/a:1019820208377, 2002.

Tipple, B. J. and Pagani, M.: The Early Origins of Terrestrial C_4 Photosynthesis, *Annu. Rev. Earth Planet. Sci.*, **35**, 435−461, doi: 10.1146/annurev.earth.35.031306.140150, 2007.

Vallet, C., Masud, Z., and Martin, M. L.: Isotopic characterization of the bioconversion of lactose into ethanol, *Food Chem.*, **63**, 115−123, doi: 10.1016/S0308-8146(97)00218-5, 1998.

van Aardenne, J. A., Dentener, F., Olivier, J. G. G., Peters, J. A. H. W., and Ganzeveld, L. N.: The EDGAR3.2 Fast Track 2000 dataset (32FT2000), Joint Research Centre, Institute for Environment and Sustainability (JRC-IES), Climate Change Unit, TP280, 21020, Ispra (Va), Italy, http://www.mnp.nl/edgar/model/v32ft2000edgar/docv32ft2000/, 2005.

van der Werf, G. R., Randerson, J. T., Giglio, L., Collatz, G. J., Kasibhatla, P. S., and Arellano Jr, A. F.: Interannual variability in global biomass burning emissions from 1997 to 2004, *Atmos. Chem. Phys.*, **6**, 3423−3441, doi: 10.5194/acp-6-3423-2006, 2006.

Yakir, D.: The paper trail of the ^{13}C of atmospheric CO_2 since the industrial revolution period, *Environ. Res. Lett.*, **6**, 034007, doi: 10.1088/1748-9326/6/3/034007, 2011.

Yamada, K., Hattori, R., Ito, Y., Shibata, H., and Yoshida, N.: Carbon isotopic signatures of methanol and acetaldehyde emitted from biomass burning source, *Geophys. Res. Lett.*, **36**, L18807, doi: 10.1029/2009GL038962, 2009.

Yamada, K., Hattori, R., Ito, Y., Shibata, H., and Yoshida, N.: Determination of carbon isotope ratios of methanol and acetaldehyde in air samples by gas chromatography-isotope ratio mass spectrometry combined with headspace solid-phase microextraction, *Isot. Env. Health Stud.*, **46**, 392−399, doi: 10.1080/10256016.2010.505686, 2010.

Yevich, R. and Logan, J. A.: An assessment of biofuel use and burning of agricultural waste in the developing world, *Glob. Biogeochem. Cyc.*, **17**, 1095, doi: 10.1029/2002gb001952, 2003.

Yokelson, R. J., Susott, R., Ward, D. E., Reardon, J., and Griffith, D. W. T.: Emissions from smoldering combustion of biomass measured by open-path Fourier transform infrared spectroscopy, *J. Geophys. Res. Atm.*, **102**, 18865−18877, doi: 10.1029/97jd00852, 1997.

Zhang, B.-L., Fallourd, V., Role, C., and Martin, G. J.: Comparison of isotopic fractionation in lactic acid and ethanol fermentations, *Bioorg. Chem.*, **31**, 227−236, doi: 10.1016/S0045-2068(03)00051-8, 2003.

Zhang, Q. L., Chang, T. L., and Li, W. J.: A Calibrated Measurement of the Atomic-Weight of Carbon, *Chinese Sci. Bull.*, **35**, 290−296, 1990.

Figures
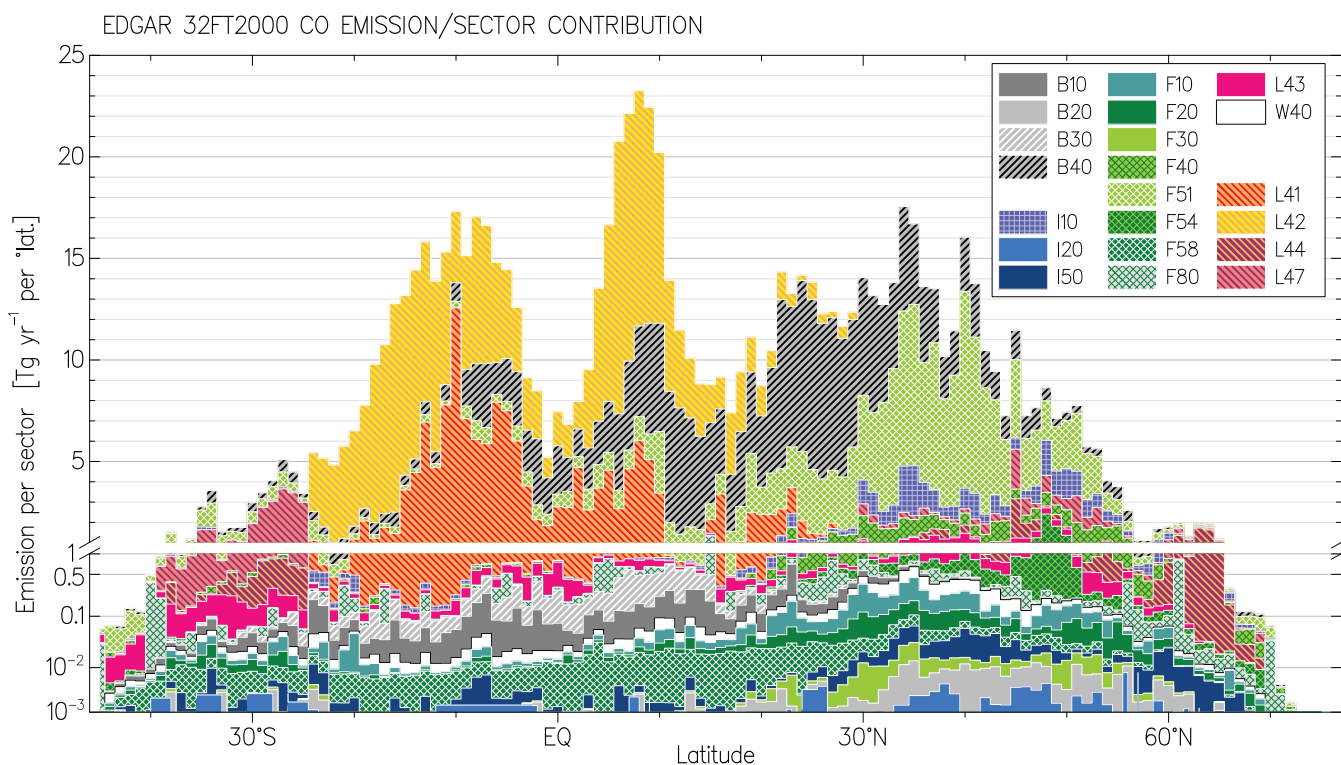
Fig. 1 Relative contributions of emission sectors to the overall emission of CO in the EDGAR inventory. Values are given in Tg(CO) yr^{-1} per degree latitude. Note: The original EDGAR biomass-burning sectors L41, L42, L44 and L47 are presented here for comparison only. They are being substituted (see text) by the GFED inventory. Mind the change in ordinate axis scale at the value of unity.
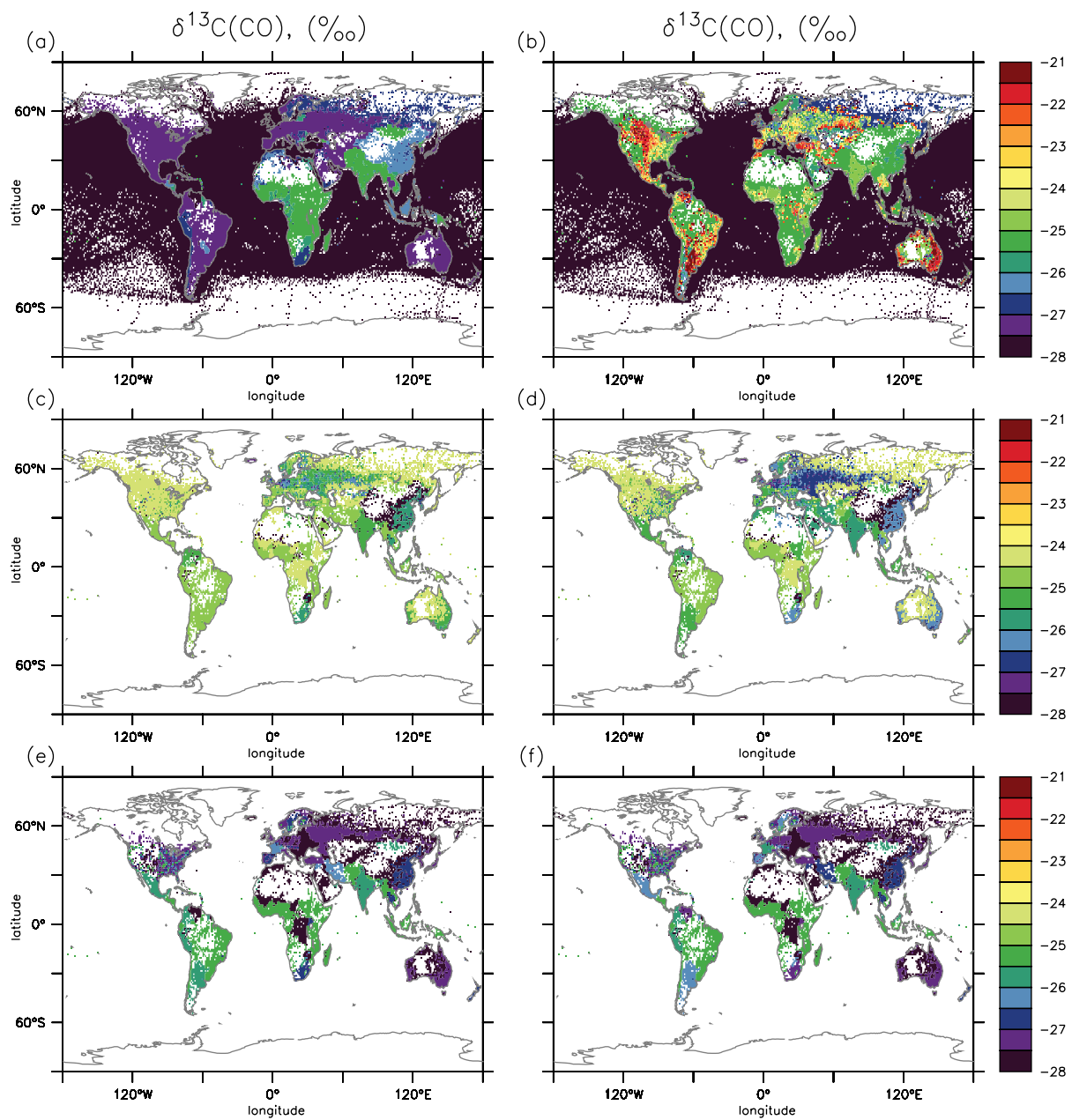
Fig. 2 Stable carbon isotope composition of CO emitted from anthropogenic sources compiled on the basis of the EDGAR FT2000 inventory. Panels (a)-(f) refer to the specific emission heights of 45, 140, 240, 400, 600 and 800 m, respectively (see text for details).
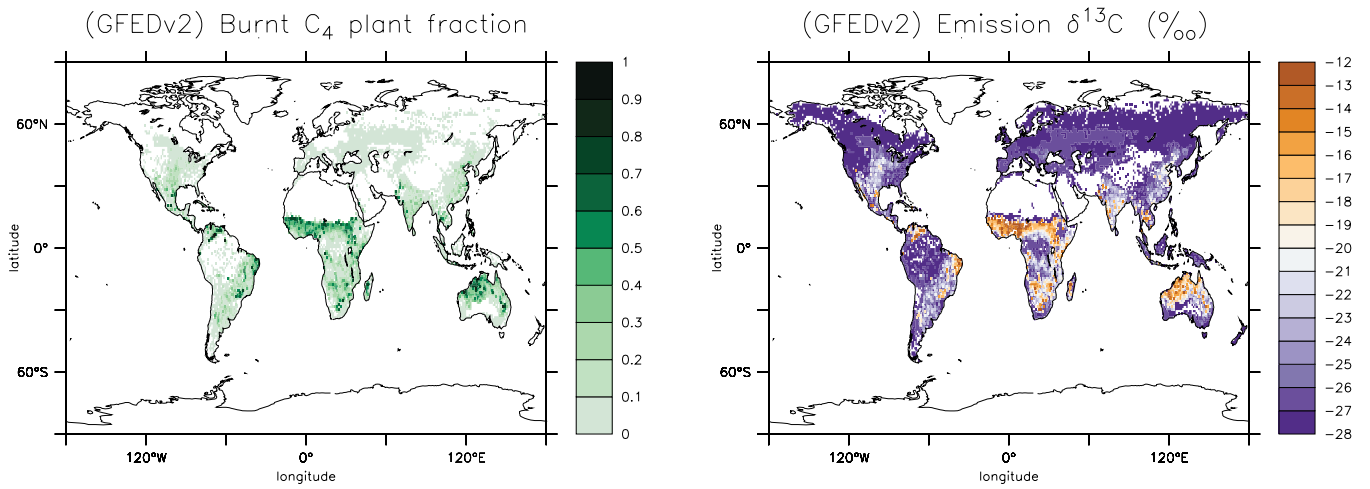
Fig. 3 Burnt biomass C_4 plant fraction (left) and corresponding isotopic signature of the emitted carbon (right) from GFED v2.1 database. Fields are "climatological" yearly averages (see text, also Fig. 4).
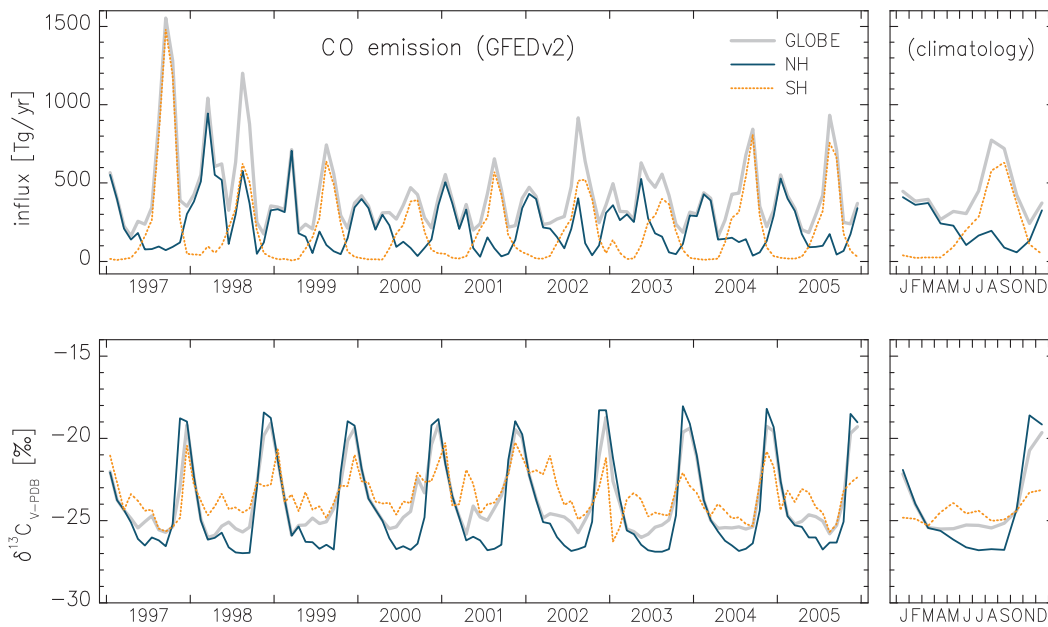
Fig. 4 Emission of CO from biomass burning sources based on the GFED v2.1 data. Upper: CO integrated flux in the northern (NH), southern hemispheres (SH) and globally. Lower: The carbon isotope composition of the respective fluxes. The right panels depict the "climatological" ensemble averages (shown in Fig. 3).
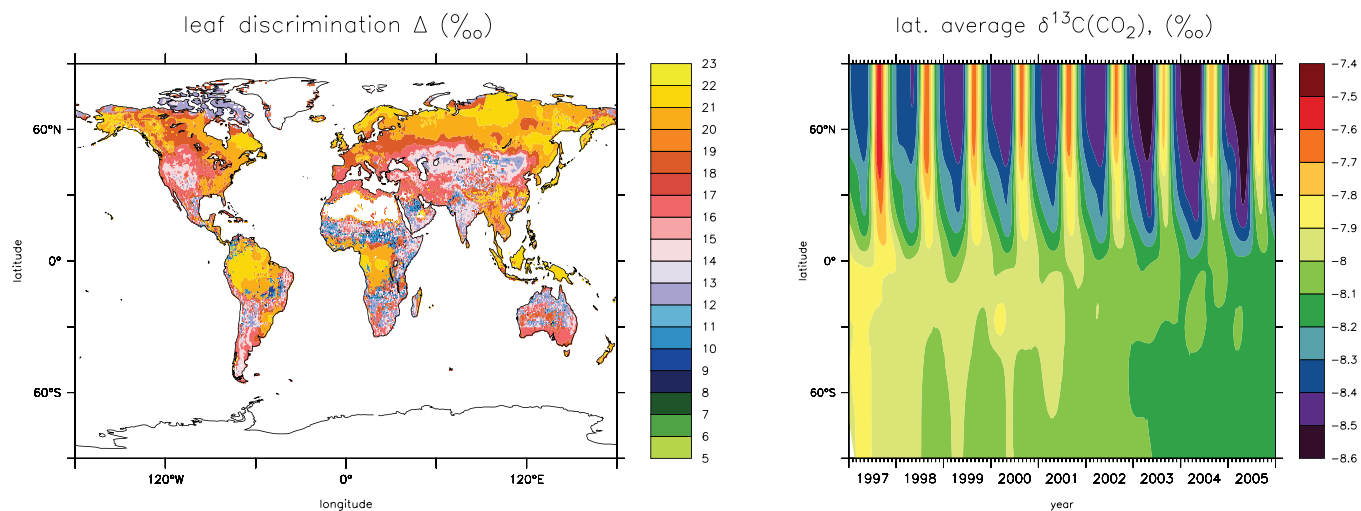
Fig. 5 Left: Global mean leaf discrimination distribution (ISOLUCP experiment, Scholze *et al.*, 2008). The distribution generally reflects the proportion of the C_3/C_4 metabolism and characteristic carbon photorespiratory fractionation in the various ecosystems, land use regimes and climate zones. Right: Time series of the latitudinal average surface isotopic composition of CO_2 from the GLOBALVIEW-CO2C13 (2009) data.
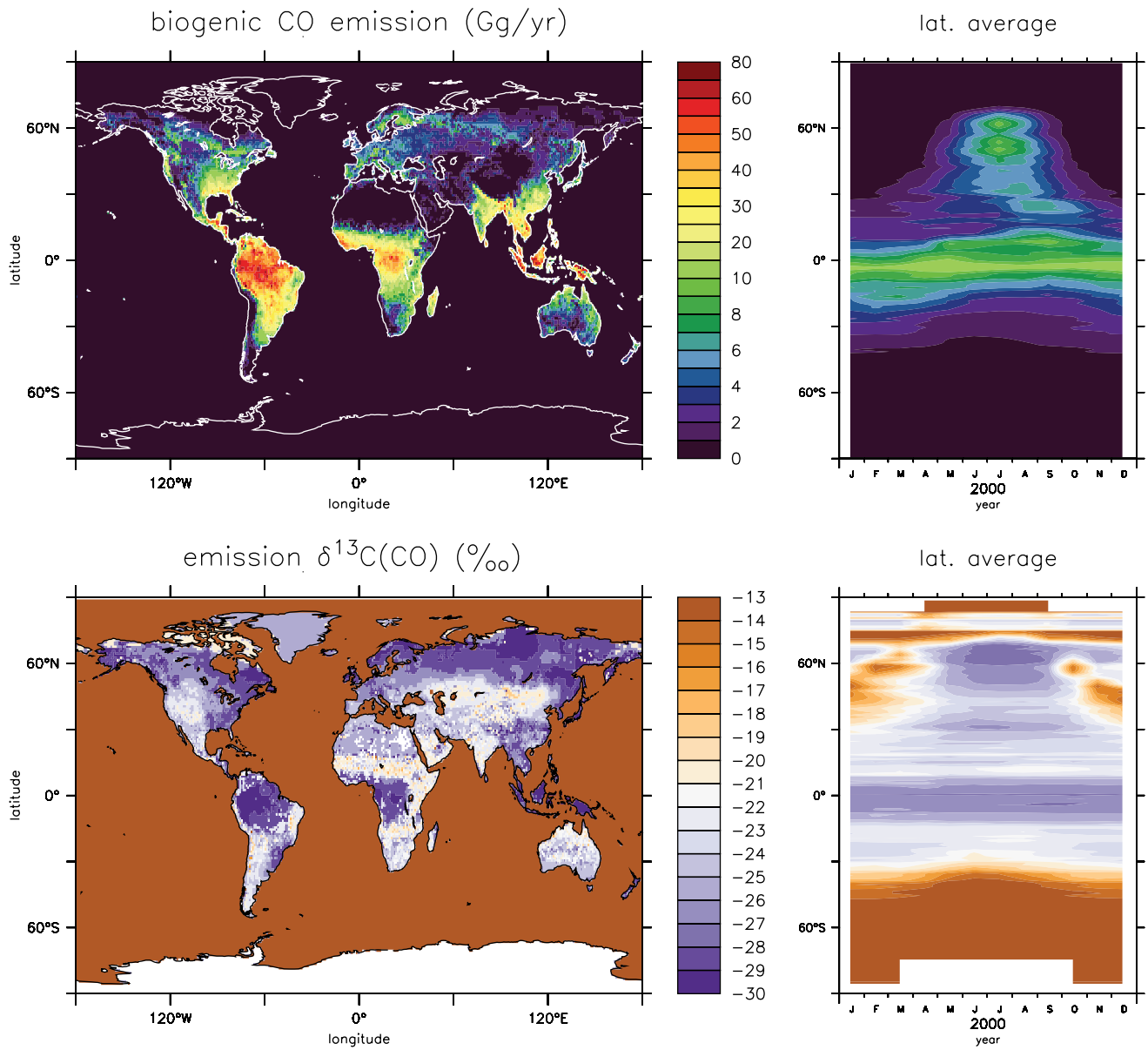
Fig. 6 Left: CO emission from the biogenic sources (upper panel) and corresponding isotopic signature (lower panel). Right: Corresponding time series of latitudinal averages for the year 2000 emission with identical colour scales.
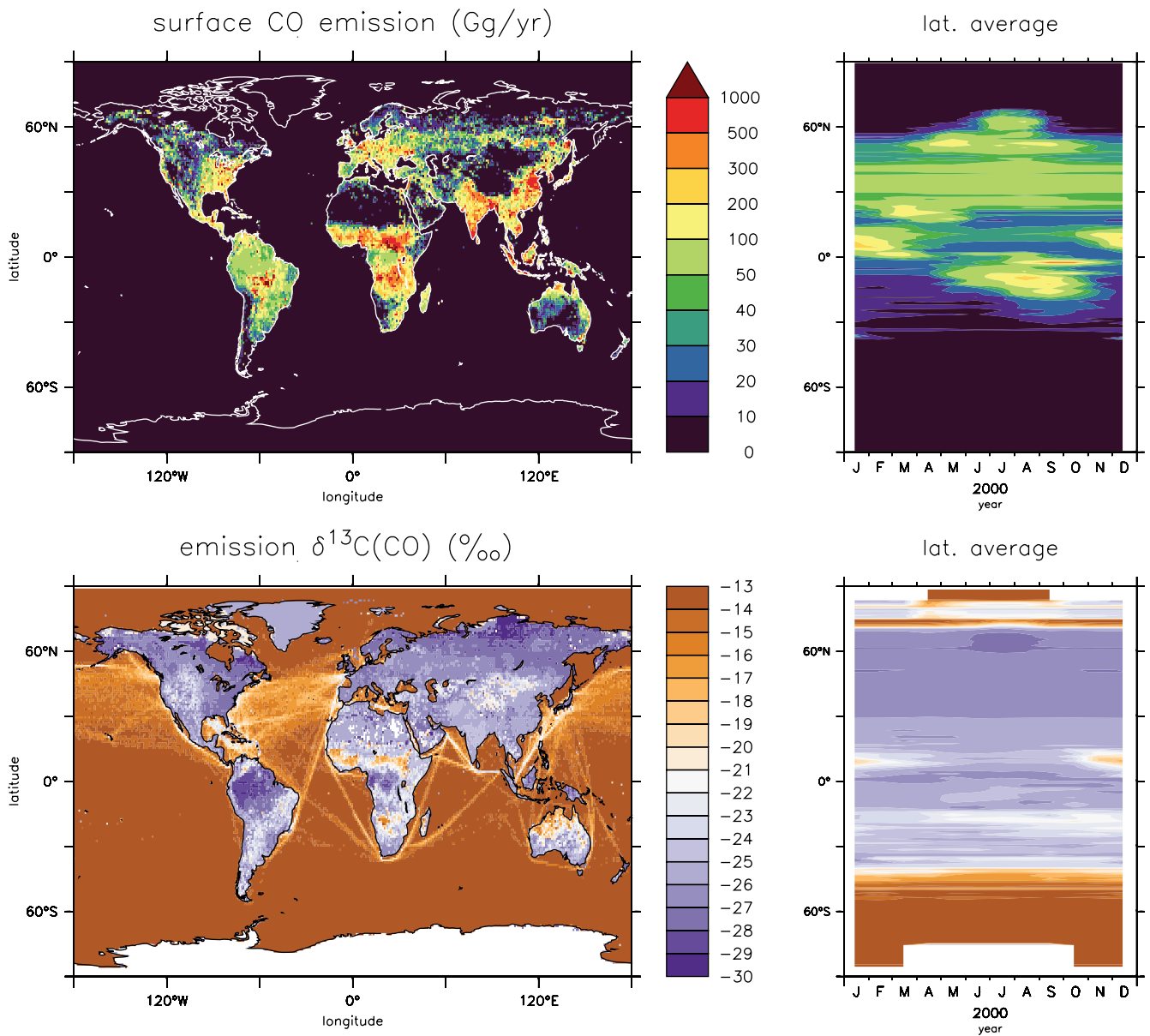
Fig. 7 Left: Annual CO emission from the surface sources (upper panel) and corresponding carbon isotopic composition (lower panel). Right: Respective time series of zonal averages for the year 2000 emission with identical colour scale.
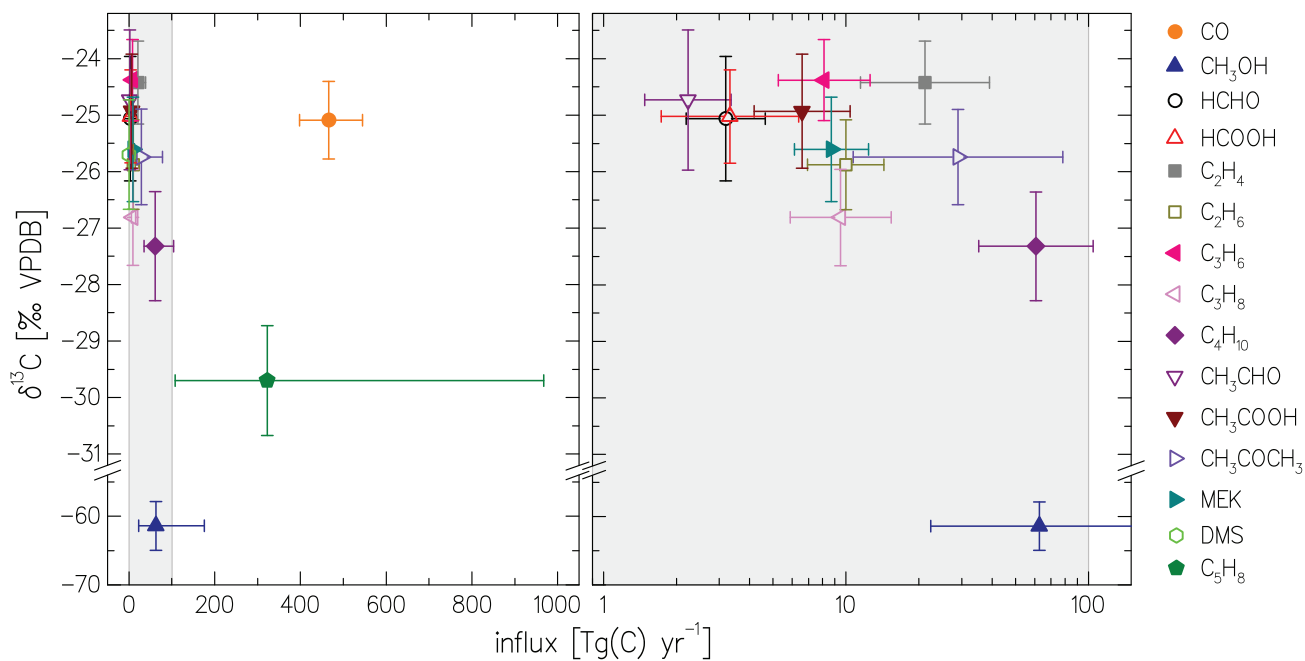
Fig. 8 Left: Overall annual surface emission isotopic compositions of the carbonaceous compounds. Right: Expanded shaded area in the
left panel for the NMHCs/VOCs. The error bars refer to the uncertainty factors from Table 5 and are discussed in Sect. 2.2.
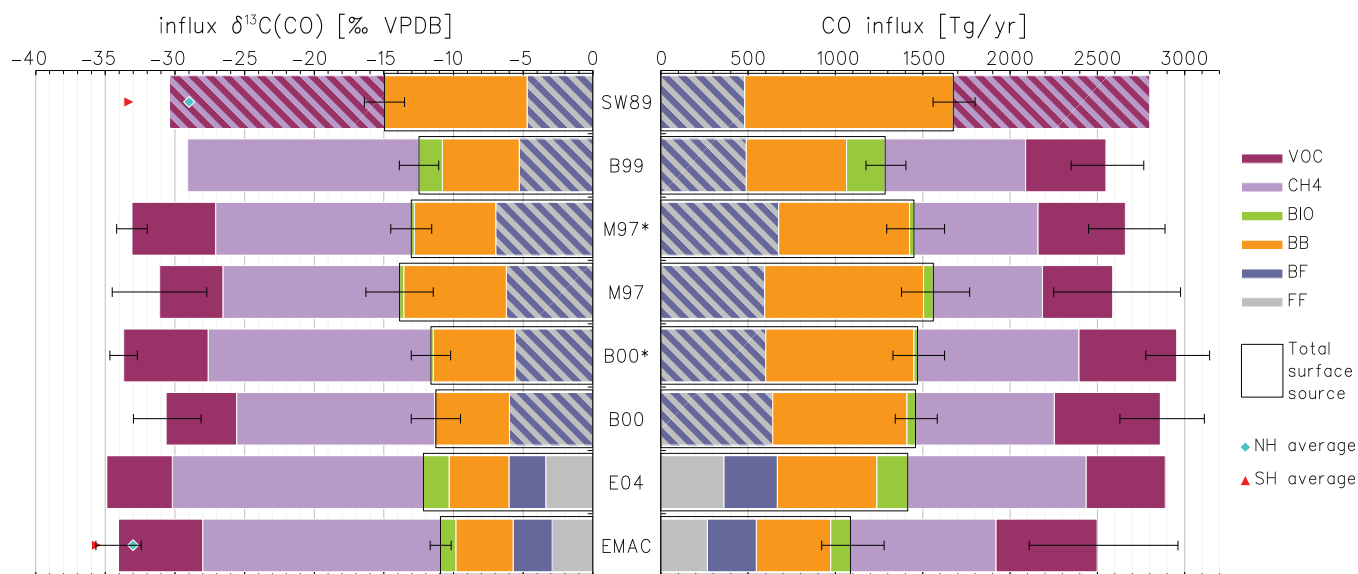
Fig. 9 Estimates of the tropospheric CO sources and their contribution to the overall source isotope composition from previous and the present studies (refers to Table 7). Abbreviations refer to: SW89 – Stevens and Wagner (1989); M97 – Manning *et al.* (1997) (case 2); B99 – Brenninkmeijer *et al.* (1999); B00 – Bergamaschi *et al.* (2000) (scenario S2); E04 – Emmons *et al.* (2004); EMAC – this study, setup based on EVAL$_2$, year 2000 (see text, Sect. 2). Asterisks denote *a priori* estimates of the corresponding inverse modelling studies.

1015   Note: Blue-grey hatched bars denote the aggregate of industrial emissions (FF and BF sources are not distinguished); SW89 report the total of photochemical sources only (light blue-violet hatched bars, respectively). Black frames denote the values for the total surface component. Right panel: Source terms by category. Left panel: Individual contribution of each source category to the overall source δ^{13}C(CO), calculated as a product of the share in total emission and respective source δ^{13}C average. Symbols denote the hemispheric tropospheric averages, where available.

Tables

Table 1 Description of EDGAR FT32 emission source sectors and associated isotopic signatures

Category	Source sectors	Emission activity	$\delta^{13}C$ [‰]
Biofuel combustion	B10, B20, B30, B40, B51	industry, power generation, charcoal production, RCO[*], road transport	−25.0 [g]
Fuel combustion, production and transmission	F10, F20, F30, F40, F51, F54, F58, F60 [d], F80, F90 [c]	industry, power generation, conversion, RCO[*], road/non-road transport, international shipping, gas production	−27.5
	F57 [a]	air traffic	−27.5 [f]
Industrial	I10, I20 [c]	iron and steel, non-ferrous metals	−27.5 [f]
	I30 [c], I60 [c], I70 [c], I90 [c], I50 [b]	chemicals, food/beverages/tobacco, solvents, misc. industry, pulp and paper	−27.5 [f]
Land use [b]	L41, L42, L44, L47	(in)direct deforestation, savannah burning, vegetation fires	− [a]
	L43	agricultural waste burning	−22.2 [e,g]
Waste [b]	W40, W50 [c]	waste incineration, misc. waste handling	−24.0 [f,g]

Notes:
[a] Excluded from the setup (or treated separately).
[b] Assuming a biomass burning-related emission source.
[c] Only CO emission (no VOCs).
[d] Only VOCs emission (no CO).
[e] For CO, a different signature of −21.3 ‰ is used (see text).
[f] Fossil source assumed.
[g] Reflects the relative contribution of C_3 and C_4 plant material.
[*] (Residential, Commercial and Other)

Table 2 Anthropogenic emission sources strengths and their isotopic signatures

Species	Source [Tg(gas) yr^{-1}]			Totals	
	Biofuel	Fossils	Waste [a]	Emission [b]	$\delta^{13}C$ [‰]
CO	250.4	280.4	16.35	547.2 / 234.6	−26.2
CH$_3$OH	6.58	3.13	0.43	10.14 / 3.80	−25.7
HCHO	3.50	0.98	0.23	4.71 / 1.88	−25.5
HCOOH	3.56	−	0.23	3.79 / 0.99	−24.9
C$_2$H$_4$	5.11	3.54	0.34	8.99 / 7.70	−26.0
C$_2$H$_6$	2.91	6.11	0.19	9.21 / 7.36	−26.6
C$_3$H$_6$	2.28	1.49	0.15	3.92 / 3.36	−26.1
C$_3$H$_8$	0.91	9.45	0.06	10.42 / 8.51	−27.2
C$_4$H$_{10}$	1.16	70.67	0.08	71.91 / 59.44	−27.4
CH$_3$CHO	2.04	−	0.13	2.17 / 1.18	−24.9
CH$_3$COOH	6.52	−	0.43	6.95 / 2.78	−24.9
CH$_3$COCH$_3$	1.89	3.18	0.12	5.19 / 3.16	−26.4
MEK	4.42	4.22	0.29	8.93 / 5.95	−26.1

Notes:
[a] Refers to the EDGAR sector L43.
[b] Values are in [Tg(gas) yr^{-1}] / [Tg(C) yr^{-1}] units, respectively.

Table 3 Biomass burning emission sources strengths and their isotopic signatures

Species	Source [Tg(gas) yr^{-1}]			Average δ^{13}C [‰]	
	NH	SH	Total [a]	NH	SH
CO [b]	223.2 (170.8−396.7)	202.8 (137.4−364.1)	425.9 (336.8−589.9) / 182.6 (144.4−252.9)	−24.0 −(23.3−25.2)	−24.4 −(23.3−25.3)
CH$_3$OH	3.17	2.98	6.15 / 2.31	−36.7	−37.1
HCHO	1.69	1.58	3.27 / 1.31		
HCOOH	1.73	1.62	3.35 / 0.87		
C$_2$H$_4$	2.47	2.32	4.79 / 4.10		
C$_2$H$_6$	1.41	1.32	2.73 / 2.18		
C$_3$H$_6$	1.11	1.04	2.15 / 1.84		
C$_3$H$_8$	0.44	0.41	0.85 / 0.69	−24.3	−24.7
C$_4$H$_{10}$	0.56	0.52	1.08 / 0.89		
CH$_3$CHO	0.99	0.93	1.92 / 1.05		
CH$_3$COOH	3.16	2.97	6.13 / 2.45		
CH$_3$COCH$_3$	0.91	0.86	1.77 / 1.08		
MEK	2.14	2.00	4.14 / 2.76		

Notes:
[a] Values are in [Tg(gas) yr^{-1}] and [Tg(C) yr^{-1}] units, respectively.
[b] For CO, interannual variation for 1997−2005 (monthly averages) is given in parentheses.

Table 4 Biogenic emission sources strengths and their isotopic signatures

Species	Sources [Tg(gas) yr^{-1}]		Totals	
	Land (Soils)	Ocean	Emission [a]	δ^{13}C [‰]
CO	100.0	12.7	112.7 / 48.3	−24.2
CH$_3$OH	151.0 [b]	–	151.0 / 56.6	−64.8
HCOOH	5.58 (1.65)	–	5.58 / 1.46	−25.4[c]
C$_2$H$_4$	10.0 (3.0)	0.91	12.13 / 5.19	−23.4
C$_2$H$_6$	–	0.54	0.54 / 0.22	−20.5
C$_3$H$_6$	2.15	1.27	3.41 / 2.92	−23.8
C$_3$H$_8$	–	0.35	0.35 / 0.29	−20.5
C$_4$H$_{10}$	–	0.40	0.40 / 0.33	−20.5
CH$_3$COOH	3.39 (1.44)	–	3.39 / 1.36	−25.7
CH$_3$COCH$_3$	40.57	–	40.57 / 24.74	−25.7
DMS	0.91	–	0.91 / 0.35	−25.7
Isoprene [d]	346.03−385.35	–	346.03−385.35 / 305.07−339.73	−28.6 to −27.2

Notes:
[a] Values are in [Tg(gas) yr^{-1}] and [Tg(C) yr^{-1}] units, respectively.
[b] Recommended updated value (Pozzer *et al.*, 2007).
[c] Corrected for emission from formicine ants (0.22 Tg yr^{-1}) of −19 ‰ (Johnson and Dawson, 1993).
[d] Calculated online.

1025

Table 5 Surface emission sources in the EMAC (EVAL$_2$ setup)

Species	Source [Tg(gas) yr^{-1}]			Aggregate uncertainty factor [a]	Totals (uncertainty)	
	Anthropogenic (incl. Biofuel)	Biomass burning	Biogenic		Emission [Tg(C) yr^{-1}] [b]	δ^{13}C [‰]
CO	547.2 (250.4)	425.9	112.7	1.17	465.6±79.1	−25.0±0.7
CH$_3$OH	10.1 (6.6)	6.15	151.0	2.81	62.7±113.2	−61.4±3.6
HCHO	4.71 (3.50)	3.27	–	1.45	3.2±1.5	−25.1±1.1
HCOOH	3.79 (3.56)	3.35	5.58	1.92	3.3±3.1	−25.2±0.8
C$_2$H$_4$	8.99 (5.11)	4.79	10.9	1.84	21.1±17.9	−25.3±0.7
C$_2$H$_6$	9.21 (2.91)	2.73	0.54	1.44	10.0±4.4	−25.9±0.8
C$_3$H$_6$	3.92 (2.28)	2.15	3.42	1.54	8.1±4.4	−24.8±0.7
C$_3$H$_8$	10.4 (0.9)	0.85	0.35	1.62	9.5±5.8	−26.8±0.9
C$_4$H$_{10}$	71.9 (1.2)	1.08	0.40	1.72	60.7±43.8	−27.3±1.0
CH$_3$CHO	2.17 (2.04)	1.92	–	1.51	2.2±1.1	−24.7±1.2
CH$_3$COOH	6.95 (6.52)	6.13	3.39	1.58	6.6±3.8	−24.9±1.0
CH$_3$COCH$_3$	5.19 (1.89)	1.77	40.6	2.71	29.0±49.6	−25.7±0.8
MEK	8.93 (4.42)	4.14	–	1.42	8.7±3.7	−25.6±0.9
DMS	–	–	1.82	3.0	0.4±0.7	−25.7±1.0
C$_5$H$_8$	–	–	365.7	3.0	322.4±644.8	−27.9±1.0

Notes:
[a] Derived from the final (composite) flux uncertainty using Eq. (12) (see Sect. 3.6).
[b] Mind the different units used for individual categories and total values, *i.e.* [Tg(gas) yr^{-1}] and [Tg(C) yr^{-1}], respectively.

Table 6 Uncertainties associated with emission sources and isotopic signatures

Category	Source	Emission (δ^{13}C signature) uncertainty [a]		
		CO	NMHCs/VOCs	Other [b]
Anthropogenic	Biofuel [c]	2 (4.6‰)	2 (4‰)	–
	Fossil fuel	1.5 (0.3‰) [d]	1.5−2.0 (2‰) [e]	–
	Waste [c]	2 (4‰)	2 (4‰)	–
Biogenic	Land (plants) [f]	3 (1.9‰)	3 (1.9‰)	3 (1.9‰)
	Ocean	2 (3.6‰) [g]	2 (2‰) [h]	–
Biomass burning		1.3 (2‰)	1.3 (2‰) [i]	–
Pseudo-emission [j]	CH$_4$	–	–	0.04 % (0.05‰) [k]
	CO$_2$	–	–	0.03 % (0.02‰)
	CH$_3$Cl	–	–	0.15 % (0.3‰) [m]

Notes:
[a] Given is the emission uncertainty factors (UFs, see Sect. 3.6) and isotopic signature uncertainty $\langle\delta_e\rangle$ (in parentheses).
[b] Values assumed for biogenic isoprene, terrestrial DMS (plant emitted), and respective pseudo-emitted species.
[c] C$_3$/C$_4$ plant composite, based on $\langle\delta^{13}C(C_3)\rangle$ = 5.7‰ and $\langle\delta^{13}C(C_4)\rangle$ = 2.5‰ (see text).
[d] From Stevens *et al.* (1972).
[e] Varies for each species due to the proportion of the fossil fuel (1.5) and industry (2.0) uncertainty factors contribution (Olivier *et al.*, 1999).
[f] The UFs are from Guenther *et al.* (1995). δ^{13}C uncertainty is derived from $\langle\delta^{13}C(CO_2)\rangle$ = 0.02‰ and leaf discrimination uncertainty of $\langle\Delta\rangle$ = 2‰. Exceptionally, methanol $\langle\delta^{13}C\rangle$ = 6.6‰ is augmented by the uncertainty of plant emission fractionation (Keppler *et al.*, 2004; Yamada *et al.*, 2010, ±6.3‰, see text).
[g] Following Manning *et al.* (1997).
[h] Based on variability in δ^{13}C of the marine carbon content from Avery Jr *et al.* (2006).
[i] Exceptionally, for methanol $\langle\delta^{13}C\rangle$ = 2.2‰ is augmented by the uncertainty of BB emission fractionation (Yamada *et al.*, 2009, ±0.8‰, see text).
[j] Quoted are mixing ratio uncertainties (not uncertainty factors).
[k] Assigned equal to the upper limit of the atmospheric variation.
[m] Error of the mean from Thompson *et al.* (2002).

Table 7 Tropospheric CO sources and their isotopic composition from the present and previous studies

Study	SW89	B99 [a]	M97 [a,b,c]	B00 [a,b,c]	E04 [a,d]	EVAL$_2$ [a,d]
Model	−	−	GFDL (2D)	TM2	MOZART2	EMAC
Emission inventories [e]	1971	1972−1998	1987−1995	1987[+]	1997−1999	2000[+]
CH$_4$ oxidation	(−55 ‰) [f]	400−1000 (−52.6 ‰)	624 (−52.6 ‰)	795 (−51.1 ‰)	1022 (−51 ‰)	834 (−51.2 ‰)
NMHC oxidation	(−32.3 ‰) [f]	200−600 (−32.2 ‰)	403 (−29.3 ‰)	607 (−23.9 ‰)	453 (−30 ‰)	579 (−26.1 ‰) [g]
Fossil fuel / Biofuel usage	480 (−27.5 ‰)	300−550 (−27.5 ‰)	595 (−27 ‰)	641 (−26.7 ‰)	361 (−27 ‰) / 306 (−25 ‰)	272 (−27.4 ‰) / 285 (−25 ‰)
Biomass burning	1195 (−24 ‰)	300−700 (−24.5 ‰)	909 (−21 ‰)	768 (−20 ‰)	570 (−21.8 ‰)	434 (−24.1 ‰)
Biogenic / Oceans		60−160 (–) / 20−200 (−13.5 ‰)	– / 57 (−13.5 ‰)	– / 49 (5.1 ‰)	158 (−32 ‰) / 20 (−12 ‰)	102 (−25.7 ‰) / 13 (−13.5 ‰)
Photochemical sources	1100−1250 (−38.4 ‰) [f]	1265 (−33.5 ‰) [h]	1027 (−43.4 ‰)	1402 (−39.3 ‰)	1475 (−44.6 ‰)	1414 (−40.9 ‰) [g]
Uncertainty	±125 (±1.7 ‰)	±180 (±3.7 ‰)	±182 (±3.5 ‰)	±127 (±2.5 ‰)	−	±420 (±4.4 ‰)
Surface sources	**1550−1700 (−25.0 ‰)**	**1285 (−24.8 ‰) [h]**	**1561 (−23 ‰)**	**1458 (−22.1 ‰)**	**1415 (−24.8 ‰)**	**1086 (−25.2 ‰)**
Uncertainty	**±125 (±1.7 ‰)**	**±238 (±1.4 ‰)**	**±207 (±2.4 ‰)**	**±125 (±1.8 ‰)**	**−**	**±194 (±0.7 ‰)**
Total sources	2800 (−30.3 ‰)	2550 (−34.9 ‰)	2588 (−31.1 ‰)	2860 (−30.5 ‰)	2890 (−34.9 ‰)	2525 (−34.1 ‰) [g]
Overall uncertainty	±250 (±2.0 ‰)	±216 (±1.4 ‰)	±389 (±3.4 ‰)	±252 (±2.4 ‰)	−	±462 (±1.6 ‰)

Notes: The source/sink terms are given in [Tg(CO) yr^{-1}] with the corresponding δ^{13}C composition [‰ V-PDB] of the sources in parentheses. Values are the tropospheric averages. Abbreviations refer to: SW89 – Stevens and Wagner (1989); M97 – Manning *et al.* (1997) (case 2); B99 – Brenninkmeijer *et al.* (1999); B00 – Bergamaschi *et al.* (2000) (scenario S2); E04 – Emmons *et al.* (2004); EVAL$_2$ – this study (see Sects. 1, 2).

[a] A "bottom-up" estimate (for the inverse modelling studies, the *a priori* setup).

[b] An inversion technique to improve the emission strengths/isotope signatures is employed.

[c] A simplified chemistry scheme (no intermediates in the CH$_4 \rightarrow$ CO chain, no NMHC chemistry) is used.

[d] A detailed chemistry scheme (*e.g.*, CH$_4$ and NMHC chemistry with intermediates and removal processes) is used.

[e] The year(s) the aggregate of the emission inventories correspond closest to; the plus signs indicate that the transient biomass burning inventory was used, with the listed year referring to the anthropogenic emissions revision.

[f] The authors assume a too high NMHC:CH$_4$ source fluxes partitioning of 5.5 based on then limited information on sources O isotope composition. The ^{13}C mass-balance and photochemical source is reanalysed here in light of current knowledge on the δ^{18}O signatures of CO sources (see, *e.g.*, B99).

[g] Upper limit, assuming δ^{13}C of emitted CH$_3$OH being similar to that of other NMHCs/VOCs (about −(26±1) ‰).

[h] The average signature results from the respective source terms (denoted as the sum) assumed within the given limits.

1030

1035